HHS Public Access

Author manuscript

Nat Biomed Eng. Author manuscript; available in PMC 2019 June 01.

Published in final edited form as:

Nat Biomed Eng. 2018 December ; 2(12): 942–954. doi:10.1038/s41551-018-0290-2.

Incorporation of macrophages into engineered skeletal muscle enables enhanced muscle regeneration

Mark Juhas[1], **Nadia Abutaleb**[1], **Jason T. Wang**[1], **Jean Ye**[1], **Zohaib Shaikh**[1], **Chaichontat Sriworarat**[1], **Ying Qian**[1], and **Nenad Bursac**[1,2,2]

[1]Department of Biomedical Engineering, Duke University, Durham, NC, USA.

[2]Regeneration Next, Duke University, Durham, NC, USA.

Abstract

Adult skeletal muscle has a robust capacity for self-repair, owing to synergies between muscle satellite cells and the immune system. In vitro models of muscle self-repair would facilitate the basic understanding of muscle regeneration and the screening of therapies for muscle disease. Here, we show that the incorporation of macrophages into muscle tissues engineered from adult-rat myogenic cells enables near-complete structural and functional repair after cardiotoxic injury in vitro. First, we show that—in contrast with injured neonatal-derived engineered muscle—adult-derived engineered muscle fails to properly self-repair after injury, even when treated with pro-regenerative cytokines. We then show that rat bone-marrow-derived macrophages or human blood-derived macrophages resident within the in vitro engineered tissues stimulate muscle satellite cell-mediated myogenesis while significantly limiting myofibre apoptosis and degeneration. Moreover, bone-marrow-derived macrophages within engineered tissues implanted in a mouse dorsal window-chamber model augmented blood vessel ingrowth, cell survival, muscle regeneration and contractile function.

Skeletal muscle possesses the unique ability to achieve complete structural and functional recovery following minor acute damage[1]. This regenerative capacity is attributed to resident stem cells known as muscle satellite cells (MuSCs). In homoeostatic muscle, quiescent MuSCs express Pax7 and reside in well-defined niches abutting myofibres—the force-generating cells in the tissue[2,3]. On injury, MuSCs become activated and asymmetrically

* nbursac@duke.edu. **Correspondence and requests for materials** should be addressed to N.B.

Author contributions

M.J. and N.B. conceived and designed the research. M.J., N.A., J.T.W., J.Y., Z.S. and C.S. performed the experiments. Y.Q. performed the implantation surgery. M.J., N.A., J.Y., Z.S. and N.B. analysed the results. M.J. and N.B. wrote the manuscript.

Competing interests

The authors declare no competing interests.

Reporting Summary. Further information on research design is available in the Nature Research Reporting Summary linked to this article.

Code availability. Custom MATLAB and ImageJ codes are available on request.

Data availability

All the data supporting the findings of this study are available within the paper and its Supplementary Information.

Additional information

Supplementary information is available for this paper at https://doi.org/10.1038/s41551-018-0290-2.

Publisher's note: Springer Nature remains neutral with regard to jurisdictional claims in published maps and institutional affiliations.

divide to selfrenew while generating pools of proliferative myogenic precursor cells (MyoPCs) capable of rebuilding damaged myofibres via cell fusion. Regulating the activity of MuSCs are orchestrated waves of pro- and anti-inflammatory factors primarily released from infiltrating circulatory macrophages helping to stimulate myogenic activation and differentiation[4–7]. Although normally robust, the regeneration process can be impaired in cases of severe muscle loss or chronic degenerative diseases, resulting in environments that prevent the generation of new muscle[8] or reduce the regenerative capacity of MuSCs[9,10].

Recent advances in tissue-engineered organs-on-chips have enabled the modelling and improved understanding of complex biological phenomena in vitro[11,12]. Specifically, various methods to recreate critical components of the muscle tissue environment in vitro have been developed to systematically study the cellular events and interactions involved in skeletal muscle repair, and to screen for potential inducers of regeneration. Artificial niches[13–15] and neonatal-derived three-dimensional (3D) engineered muscle tissues[16] have proven capable in modelling MuSC quiescence, selfrenewal or response to injury. In such biomimetic systems, the physical interactions between the MuSCs, myofibres and extracellular matrix (ECM) have been replicated; however, the critical roles of the immune cells have not been considered.

Here, we show that incorporating bone-marrow-derived macrophages (BMDMs) into adult-derived 3D muscle cell cultures (constructs) enables near-complete tissue repair following significant cell damage in vitro. Within this biomimetic environment, resident BMDMs support patterns of MuSC proliferation and differentiation consistent with natural muscle repair post-injury, while their absence results in a depletion of the MuSC pool and progressive muscle degeneration. Notably, the BMDMs significantly limit myofibre apoptosis and attenuate the pro-inflammatory environment induced by muscle damage. Comparative studies of neonatal- and adult-derived engineered muscle further suggest that the discrepancy in regenerative capacity[16] may be attributed to a greater propensity towards apoptosis post-injury in the adult-derived cells. Similar to rat BMDMs, human blood-derived macrophages (hMacs) enable self-repair of engineered muscle, supporting the robustness of the model. In vivo, the presence of BMDMs within engineered muscle implants enhances blood vessel ingrowth, cell survival and contractile function. Together, our results provide a 3D culture system for studies of muscle–immune cell interactions and suggest a strategy to enhance the regenerative potential of engineered tissues.

Results

Engineering adult-derived rat skeletal muscle tissues.

Cylindrical skeletal muscle tissue constructs were engineered using expanded adult-derived rat MyoPCs differentiated in 3D hydrogel culture (Fig. 1a and Supplementary Fig. 1). Before 3D culture, MyoPCs were expanded in the presence of basic fibroblast growth factor (bFGF) for up to 5 passages, during which they experienced a decline in the $Pax7^+$ cell fraction but still contained significant numbers of activated myogenic cells (Pax7: 23.1 ±4%; MyoD: 62.8 ±8%) and differentiated myoblasts (myogenin (MyoG): 14.6 ±3%) (Fig. 1b). MyoPCs were then embedded in a mixture of fibrin gel and 20% *v/v* Matrigel and cultured dynamically on a rocker (±30 ° tilt, 0.4 Hz)[17]. Following 10 d of culture, the engineered

muscle maintained a pool of undifferentiated $Pax7^+$/M-cadherin$^+$ muscle stem cells (MuSCs) and aligned, multi-nucleated and striated myofibres surrounded by a basal lamina-like matrix (Fig. 1c). Along with the biomimetic architecture, the contractile force output of these adult-derived muscle tissues (twitch: 25.1 ±0.9 mN mm^{-2}tetanus: 33.4 ±0.7 mN mm^{-2}; Fig. 1d) approximated those measured in neonatal-derived engineered[16,17] and native neonatal[18] muscles. However, unlike neonatalderived engineered muscles[16], the adult-derived constructs were unable to regenerate muscle fibres (Fig. 1e) or sarcomeric structures (Supplementary Fig. 2a) following injury induced by exposure to cardiotoxin (CTX). To non-invasively assess the extent of initial CTX injury and further monitor functional recovery of injured constructs with time of culture, we transduced expanded MyoPCs with a lentivirus-encoding calcium (Ca^{2+}) indicator, GCaMP6 (ref. [19]), driven by a muscle-specific promoter, MHCK7[20,21]. Every 2–3 d after CTX exposure, electrically induced Ca^{2+} transients reported by GCaMP6 were recorded in a live imaging chamber and their amplitude was found to significantly decrease at the time of injury and not recover during the subsequent 15 d of culture (Supplementary Fig. 3a,b). Interestingly, chronic post-injury supplementation of the known pro-regenerative factors insulin-like growth factor 1 (IGF-1; ref. [22]), interleukin-10 (IL-10; ref. [23]) or granulocyte colony-stimulating factor (G-CSF)[24] did not prevent the loss of myofibres (Supplementary Fig. 2a) or Ca^{2+} transient amplitude (Supplementary Fig. 3b), and only slightly promoted the recovery of contractile force generation by 10 d post-injury (to less than 8% of pre-injury values; Fig. 1f).

Engineering adult-derived rat muscle–BMDM constructs.

Given the significant roles of immune system cells—and in particular the monocyte/macrophage lineage—in adult skeletal muscle regeneration[4–7], we sought to incorporate BMDMs within engineered muscle in attempt to enhance its self-repair capacity. BMDMs were derived through two-dimensional (2D) culture of primary marrow cells in macrophage colony-stimulating factor (M-CSF)-supplemented media[25,26], and 3D co-cultured with expanded MyoPCs to form muscle–BMDM (Mu–BMDM) constructs (Fig. 2a). Expression of CD68 in nearly all cells (98.3 ±0.8%) in 2D culture suggested efficient macrophage differentiation, while high levels of CD206 (83.3 ±6%) and limited inducible nitric oxide synthase expression (4.9 ±1%) suggested the acquisition of a primarily anti-inflammatory phenotype (Supplementary Fig. 4a,b), consistent with previous studies of M-CSF-driven BMDM differentiation[26,27]. Within the 3D Mu–BMDM constructs, macrophages were distributed alongside myofibres throughout the whole tissue (Fig. 2b) where they retained the predominant expression of anti-inflammatory markers (Supplementary Fig. 4c) and attained a density (Supplementary Fig. 4d) comparable to that found after CTX injury in native mouse muscle[28]. Compared with muscle-only (Mu-only) constructs, incorporation of the BMDMs did not alter the distribution (Fig. 2c) or density of MuSCs (6.5 ±1% of all nuclei), reduce tissue contractile function (Fig. 2d), or affect early muscle formation or fusion events (Supplementary Figs. 5 and 6).

Regenerative ability of Mu–BMDM constructs.

Live GCaMP6 imaging following CTX injury in Mu-only and Mu–BMDM constructs (Fig. 2e) showed that both tissues exposed to CTX lost ~75% of the Ca^{2+} transient signal (Mu-only: 24 ±2%; Mu–BMDM: 23 ±1% of the pre-CTX level). While signal amplitudes in Mu-

only constructs steadily decreased with time post-injury (to 12 ±1% of the pre-injury value at 15 d post-CTX), Mu–BMDM constructs showed progressive recovery of the signal to levels that by 10 d postinjury approached non-injured controls (85 ±4% of the pre-injury value at 15 d post-CTX; Fig. 2e,f and Supplementary Video 1). To assess whether macrophage phenotype was required for the observed functional recovery, we replaced BMDMs in 3D constructs with rat bone-marrow-derived mesenchymal stem cells (BMDMSCs) obtained by a standard 2D culture protocol[29] without M-CSF supplementation. While yielding a slightly greater functional recovery than was found in Mu-only constructs, the addition of BMDMSCs was significantly less effective compared with the addition of BMDMs (Fig. 2f).

Consistent with the Ca^{2+} transient results, Mu–BMDM constructs exhibited gradual recovery of muscle mass over the 15 d postCTX period compared with a steady decrease in muscle area and nuclei numbers found in Mu-only constructs (Fig. 3a–c). Similar to Mu-only injury (Fig. 1e), Mu–BMDM constructs exposed to CTX underwent immediate myofibre fragmentation (Supplementary Fig. 4d); however, this initial damage was followed by robust myofibre recovery without changes in BMDM numbers relative to pre-injury levels (Supplementary Fig. 4d,e). Concurrent with the muscle regrowth, tetanic force production of the Mu–BMDM constructs steadily improved over the 15 d period while drastically decreasing in the Mu-only group (Fig. 3d). Importantly, similar to neonatal-derived engineered muscle[16], regenerated myofibres within adult-derived Mu–BMDM constructs experienced successful reformation of registered sarcomeric structures (Fig. 3e).

Considering the known effects of macrophages on in vivo MuSC activation, proliferation and differentiation[4–7], we further assessed the myogenic process in injured muscle constructs by tracking the cellular expression of the myogenic markers Pax7, MyoD and MyoG and the proliferation marker Ki67 (Fig. 3f,g and Supplementary Fig. 7). Since the CTX injury did not deplete $Pax7^+$ MuSCs (Supplementary Fig. 8), Mu–BMDM and, to a lesser extent, Mu-only constructs experienced an early myogenic response evidenced by increased fractions of $Pax7^+$, $Ki67^+$ and $MyoD^+$ cells at 5 d post-injury, which marked the proliferation of an otherwise quiescent MuSC pool (Fig. 3f,g and Supplementary Fig. 7b,c). In Mu–BMDM constructs, this was followed by a drop in the $Pax7^+$ cell fraction towards preCTX levels and recovery of $MyoG^+$ cell numbers (Fig. 3g), signifying myogenic differentiation and rebuilding of myofibres through the addition of new myonuclei. In contrast, in Mu-only tissues, the $Pax7^+$ cell fraction significantly decreased compared with pre-CTX levels and was accompanied by a steady loss of $MyoG^+$ cells (Fig. 3g). To further assess the cell dynamics post-injury, we supplemented EdU into the media every day following CTX exposure, cumulatively marking proliferative cells. In both Mu-only and Mu–BMDM constructs, significant proliferative events were already observed at day 2 post-injury (Supplementary Fig. 9a,b). In agreement with myogenic marker assessment, cells within Mu–BMDM constructs continued to proliferate to 5 d post-CTX injury before levelling off (Supplementary Fig. 9a,b), consistent with MuSC proliferation and subsequent differentiation or reversion towards quiescence. In contrast, Mu-only tissues exhibited a steady decline of EdU^+ cells over 15 d post-CTX (Supplementary Fig. 9a,b), suggesting loss of the proliferative cells. Furthermore, the EdU^+ nuclei in Mu–BMDM constructs resided in

either myofibres or MyoD^{+}, but rarely vimentin^{+} cells (Supplementary Fig. 9c–e), suggesting that the majority of the proliferating cells post-injury were myogenic.

Effect of BMDMs on preventing cell apoptosis following CTX injury.

The observed pattern of initial MuSC proliferation, but ultimate decline over 15 d, in CTX-injured Mu-only constructs (Fig. 3c,f,g, Supplementary Fig. 7a and Supplementary Fig. 9a,b) prompted us to assess the potential roles of BMDMs in preventing cellular death after injury in addition to enhancing myogenesis. Significantly higher levels of activated (cleaved) caspase-3—a marker of skeletal muscle apoptosis[30]—were found in Mu-only compared with Mu–BMDM constructs (Fig. 4a,b). In Mu-only constructs, apoptotic events began by day 2 post-injury and lasted until day 10, in contrast with Mu–BMDM tissues where apoptosis rapidly resolved 2–5 d post-injury (Fig. 4a,b). To establish whether the anti-apoptotic effect of BMDMs was the governing factor in Mu–BMDM regeneration, we explored pan-caspase inhibition— a strategy known to support muscle survival and regeneration in vivo[31,32]. Specifically, a pan-caspase inhibitor, Q-VD-OPh[32], was applied to Mu-only constructs for the first 10 d post-injury, thus avoiding the potential adverse effects on late-stage myogenesis[31,33]. Application of the inhibitor rescued the decline in Ca^{2+} transient amplitude (Fig. 4c,d) and attenuated apoptotic events, as evidenced from the decreased expression of cleaved caspase-3 and increased muscle area in Mu-only cross-sections (Fig. 4e). Further comparisons of tetanic force, total myofibre area, cleaved caspase-3 area and EdU^{+} cell density in Q-VD-OPh-treated Mu-only versus Mu– BMDM constructs (Fig. 4f) suggest that the pro-regenerative effects of BMDMs on engineered muscle may be largely attributed to their anti-apoptotic action.

Paracrine action of BMDMs following CTX injury.

Next, we sought to determine whether the anti-apoptotic effects of BMDMs following injury were mediated through paracrine signalling or only via cell-contact-mediated mechanisms, which has been previously reported[34,35]. Therefore, we performed a shared-media assay by culturing paracrine Mu-only (P-Mu-only) and paracrine Mu– BMDM (P-Mu–BMDM) constructs in the same well. Interestingly, following ‘severe’ CTX injury (~75% reduction in the GCaMP6 signal), neither of the two constructs was able to recover (Fig. 5a), which was further evident from tetanic force measurements at 15 d post-CTX (Fig. 5b) and steady degeneration of myofibres with time post-injury (Fig. 5c,d). Next, we applied a ‘mild’ injury condition (~50% reduction in the GCaMP6 signal) to assess whether this lack of regeneration in the paracrine setting is dependent on the severity of injury. In the mild injury condition, the GCaMP signal recovered in both P-Mu–BMDM and P-Mu-only constructs in the paracrine setting, but not in Mu-only constructs (Fig. 5e). This was associated with significant increases in tetanic force recovery at 15 d post-CTX (Fig. 5f) and steady regrowth of myofibres with time post-injury (Fig. 5g,h). Consistent with the results in the severe injury condition, the lack of recovery from mild injury in Mu-only constructs was associated with the significantly increased apoptosis by day 5 post-CTX, in contrast with the attenuation of apoptosis observed in P-Mu-only and P-Mu–BMDM constructs (Supplementary Fig. 10a,b).

The shared-media assays suggested a significant role of secreted factors in both muscle degeneration and BMDM-mediated repair. Specifically, the results implied a release of pro-apoptotic cytokines by damaged muscle and—depending on the severity—the ability of BMDMs to attenuate or counteract this response and create a proregenerative environment to support muscle regrowth. In an attempt to better understand this paracrine cross-talk, culture media conditioned by Mu-only and Mu–BMDM tissues were analysed using a quantitative cytokine array before and 2, 5, 10 and 15 d after severe CTX injury (Fig. 6a and Supplementary Fig. 11). Compared with Mu-only constructs, the Mu–BMDM constructs showed decreased secretion of the pro-inflammatory factors interferon gamma (IFNγ), interleukin-1β (IL-1β) and tumour necrosis factor-α (TNFα). In particular, IL-1β and TNFα (cytokines associated with muscle apoptosis[36–40]) remained significantly elevated to day 10 post-injury in Mu-only but not Mu–BMDM tissues, while the secretion of monocyte chemoattractant protein-1 (MCP-1; also referred to as CCL-2) remained similar in the two groups. Concurrently, media levels of IL-10 and interleukin-6 (IL-6)—two cytokines linked to inhibition of IL-1β and TNFα secretion[41–43]—were significantly increased in the presence of BMDMs (Fig. 6a and Supplementary Fig. 11). Although the anti-inflammatory action of IL-10 is known to support muscle repair[23,44], the effects of IL-6 can vary[45,46], warranting more detailed studies in the future. Together, these temporary cytokine profiles suggested important roles of macrophages in the resolution of muscle injury-induced pro-inflammatory milieu. Analysis of gene expression in Mu–BMDM constructs further supported this notion as the expressions of Lcn2 and Arg1 (pro- and anti-inflammatory markers, respectively[47]) were both upregulated at day 2 post-CTX, yet only Arg1 levels remained elevated by day 5 post-CTX (Supplementary Fig. 12a). Comparisons between the gene expressions in BMDM-only (containing only BMDMs; Supplementary Fig. 12b) and Mu-only (Supplementary Fig. 12c,d) constructs suggested that the post-CTX gene expression dynamics in Mu–BMDM tissues—particularly Arg1 levels—could be primarily attributed to macrophages responding to muscle injury.

As TNFα has been linked to caspase-dependent apoptosis[48], as well as muscle loss in chronic disease and sarcopenia[39,49], we treated Mu-only constructs with small molecule inhibitors of TNFα (Supplementary Fig. 13). Doses of 5 μ M SPD304 (ref. [50]) showed a significant increase in GCaMP signal (Fig. 6b), force generation and myofibre area (Fig. 6c), as well as a decrease in cleaved caspase-3 expression (Fig. 6d). Since TNFα, among other pro-inflammatory cytokines, stimulates MuSC activation and proliferation following injury in native muscle[51,52], we assessed whether TNFα inhibition by SPD304 had adverse effects on the myogenic process post-injury. Indeed, significantly reduced $Pax7^{+}/Ki67^{+}$ and EdU^{+} cell counts (Supplementary Fig. 14) indicated that SPD304 blunted the proliferative response of MuSCs, thus leading to only a limited regenerative response of the treated constructs (Fig. 6b,c).

Comparison with the regenerative response of neonatal-derived engineered muscle.

We previously showed that functional muscle constructs generated from neonatal myogenic cells successfully recover in response to in vitro CTX injury without the need for BMDMs[16]. While this difference between adult- and neonatalderived tissues may be attributed to a loss of regenerative potential with in vitro passage[15,53], age[54] or the

significantly lower fraction of MuSCs within the adult constructs (neonatal: 12%[16]; adult: 7% $Pax7^+$ cells), we examined other potential factors, including recently reported age-dependent differences in MuSC expression of collagen VI, tenascin-C and fibronectin[55]. However, we found no significant difference in the expression of these ECM proteins and genes before (Supplementary Fig. 15a,b) or after (Supplementary Fig. 15d) CTX injury in neonatal versus adult tissues. Considering the occurrence of pronounced apoptosis following injury in adult tissues (Fig. 4), we assessed apoptotic events in neonatal-derived muscle and found significantly lower cleaved caspase-3 expression (Supplementary Fig. 16a–c) and TUNEL staining (Supplementary Fig. 16d,e), suggesting a reduction in programmed cell death post-injury. (Supplementary Fig. 16f), suggesting that adult cells were more Furthermore, expression of the death receptor genes *FAS* and susceptible to injury-induced apoptosis, as previously reported for *TNF* was significantly lower in neonatal versus adult constructs aging muscle[39,56,57].

Human macrophages rescue the regenerative capacity of engineered rat muscle.

To further validate the robustness and translational relevance of our results, we replaced rat BMDMs with hMacs (Supplementary Fig. 17a) to generate Mu–hMac constructs (Supplementary Fig. 17b,c). On CTX injury, hMacs within these constructs supported functional recovery of injured rat muscle cells in a comparable fashion to rat BMDMs (Supplementary Fig. 17d). Furthermore, functional recovery of Mu–hMac tissues was associated with a significant increase in muscle fibre area and total nuclei, as well as a reduction of cleaved caspase-3 expression similar to the results obtained for Mu–BMDM tissues (Supplementary Fig. 17e–g). The markedly lower caspase expression in Mu–hMac compared with Mu-only constructs (Mu-only: 33.34 ±5.9; Mu–hMac: 6.17 ±1.4 μm^2 nuclei $^{-1}$ at day 5 post-CTX) suggests that, similar to rat BMDMs, the hMacs had profound effects on the reduction of apoptotic events.

Effects of BMDMs on engineered muscle vascularization, function and survival in vivo.

Regarding the robust regenerative response of injured Mu–BMDM constructs in vitro, we utilized the dorsal skinfold window-chamber model to non-invasively (in real time) track the survival, function and vascularization of engineered muscle in vivo[16]. The Mu-only and Mu–BMDM constructs were implanted after 10 d of in vitro culture and assessed intravitally every 2–3 d and ex vivo at 5, 10 and 15 d post-implantation. Previously, we reported that within window chambers constructs undergo injury early after implantation, probably due to the transition from dynamic in vitro conditions to an ischaemic avascular environment with single-sided diffusion access[16]. Intravital imaging through the chamber window revealed significantly greater vascular ingrowth in Mu–BMDM than Mu-only implants by post-implantation day 10 (Fig. 7a), which was further confirmed by CD31 immunostaining of explanted tissues (Fig. 7b–d). Video recordings of red blood cell flow verified that the ingrown vessels were functional and perfused by host blood (Supplementary Video 2). We also labelled implanted constructs with GCaMP6 to perform intravital fluorescence recordings of spontaneous Ca^{2+} transients, which exhibited significantly higher amplitudes in Mu–BMDM than Mu-only implants starting at post-implantation day 10 (Fig. 7e,f and Supplementary Video 3). Consistent with the intravital results, amplitudes of electrically induced tetanic force and Ca^{2+} transients in muscle explants (Supplementary Video 4) were

higher in the Mu–BMDM than Mu-only group at 15 d post-implantation (Fig. 7g,h), and were significantly increased from post-implantation day 5 to 15 in the Mu–BMDM but not the Mu-only implants (Fig. 7g,h).

Furthermore, we assessed whether the enhanced vascularization and function of Mu–BMDM implants was associated with improved regeneration of myofibres (Fig. 7i). Consistent with our previous observations of early injury in window-chamber implants[16], myofibre area at day 5 post-implantation in both Mu-only and Mu–BMDM tissues was significantly reduced compared with preimplantation levels (Fig. 7i,j). In agreement with the functional results, muscle mass in Mu–BMDM implants steadily recovered to approach pre-implantation levels and became significantly higher than in Mu-only implants, which showed no sign of recovery by day 15 post-implantation (Fig. 7i,j). Notably, cleaved caspase-3 levels were significantly higher in the Mu-only implants than the Mu–BMDM implants (Supplementary Fig. 18), suggesting the existence of similar degenerative and regenerative mechanisms to those described after CTX injury in vitro.

Discussion

Adult skeletal muscle is one of the most regenerative organs of the body, with MuSCs being the primary source of growth and repair[1,3]. In our adult-rat-derived engineered muscle constructs, the myogenic cell milieu of native muscle has been mimicked by the presence of both functional MuSCs and their niche constituents, as well as aligned mature myofibres and basal lamina proteins. Although the abundance of MuSCs in these constructs (~7% of nuclei) was similar to or higher than that of native adult muscles[58], injury by CTX did not lead to any appreciable muscle repair; instead, it triggered a progressive degenerative process that could not be rescued by chronic administration of established pro-regenerative cytokines. Given the critical roles of immune system cells in regulating MuSC function during skeletal muscle repair[4–7], we engineered a homoeostatic 3D co-culture environment in which adult-rat BMDMs resided within biomimetic muscle tissues. In this system, orchestrated anti-apoptotic and pro-myogenic secretory actions of resident macrophages recreated the natural regenerative response to support robust self-repair of injured engineered muscle in vitro and in vivo.

Notably, in our previous study[16], functional muscle constructs generated from neonatal rat myogenic cells successfully regenerated after in vitro CTX injury without the need for macrophage incorporation. Recently, it was reported that foetal mouse MuSCs have higher self-renewing and regenerative capacity than their adult counterparts. This was partly attributed to age-dependent differences in the expression of ECM proteins, including tenascin-C, fibronectin and collagen VI[55]. By comparing neonatal-[16] and adultderived Mu-only constructs, we found no significant difference in their kinetics of myogenesis during early differentiation and postCTX injury or in the expression levels of two out of the three ECM proteins (Supplementary Fig. 15b). This discrepancy from previous studies might result from: (1) the use of neonatal versus foetal cells (with a previous study[55] showing that MuSCs derived from day 7 neonatal muscle had gene expression more similar to adult than foetal MuSCs); (2) the effects of in vitro culture on MuSCs[15,53]; (3) potential species

differences (rat versus mouse); and (4) the fact that our gene expression analyses were performed on intact engineered muscle tissues rather than freshly isolated $Pax7^+$ MuSCs[55].

Overall, while a larger pool or a distinct phenotype of $Pax7^+$ cells could contribute to the superior regenerative capacity of neonatal- versus adult-derived constructs in our study, the higher resistance to apoptotic death of neonatal muscle cells (Supplementary Fig. 16) appeared to be the main reason for their robust recovery after injury. In contrast, the lower resistance to apoptosis and decreased regenerative capacity of adult-derived tissues could be rescued by the antiapoptotic and pro-myogenic actions of supplemented BMDMs. In particular, anti-apoptotic effects of macrophages played critical roles in preventing loss of muscle mass and function and supporting regeneration, as revealed by the fact that the pan-caspase inhibitor Q-Vd-OPh yielded similar structural and functional repair to that caused by incorporating BMDMs (Fig. 4f). While pan-caspase inhibition may have complex effects on muscle regeneration[33], it served to preserve the number and integrity of myofibres—essential components of the functional MuSC niche[3]—which in turn supported the efficient MuSC response to injury, leading to robust myogenic repair.

In previous studies, anti-apoptotic effects of macrophages on injured muscle arose via cell-contact-mediated mechanisms[34,35]; yet, in our study, significantly reduced muscle apoptosis in the presence of BMDMs (Fig. 4a,b) was at least in part contributed by macrophage paracrine action that downregulated the expression of the pro-inflammatory cytokines TNFα and IL-1β (Fig. 6a) known to associate with muscle wasting and degeneration[36–39,59,60]. Still, a proinflammatory environment induced by injury in vivo is required to stimulate MuSC proliferation and myogenic repair[51,52,61], while the subsequent switch to an anti-inflammatory milieu is essential for completing tissue regeneration[4,5,7]. Consistent with this process in vivo, the BMDMs within the injured engineered muscle experienced a transient upregulation of the pro-inflammatory marker Lcn2 early after injury, yet continued to upregulate the anti-inflammatory marker Arg1, suggesting conversion from a pro-inflammatory phenotype towards an anti-inflammatory phenotype by day 5 postCTX (Supplementary Fig. 12). The sustained anti-inflammatory environment, marked by continual expression of IL-10 out to day 10 post-CTX, may have aided injury resolution and successful regeneration of Mu–BMDM tissues[23]. Still, given the limited number of markers studied, further work is needed to better characterize injury-induced changes in macrophage phenotype within the 3D engineered muscle environment.

We also utilized window-chamber implantation as an in vivo injury model (with initial cell damage resulting from a hypoxic environment), which uniquely allowed repeated intravital assessments of implanted tissue survival, function and vascularization. Similar to in vitro studies, engineered muscle implants with incorporated BMDMs showed reduced apoptotic events (Supplementary Fig. 10) and enhanced cell survival, myogenesis and function (Fig. 7). Since macrophages support angiogenesis and vascular remodelling during development and injury in many organs, including muscle[7,62], it was not surprising that incorporated BMDMs within the muscle implants would also accelerate vascular ingrowth (Fig. 7a–c), probably by their secretion of angiogenic factors[63] and direct interactions with vascular sprouts[64]. Notably, the onset of functional recovery in vitro (Fig. 3d) was faster compared with in vivo (Fig. 7h), where significant regeneration occurred only after 10 d post-

implantation, consistent with our previous window-chamber study[16]. This difference might be attributed to different causes of injury; namely, CTX in vitro versus ischaemia in vivo, which agrees with previous mouse studies showing significantly faster muscle regeneration after CTX than ischaemia–reperfusion injury[65]. The accelerated functional recovery past 10 d in vivo coincided with the establishment of robust muscle perfusion (and probably the resolution of ischaemia), as previously reported[66].

In summary, introducing BMDMs within functional engineered muscle presented components of the systemic environment to a local niche of myogenic cells—a strategy that enabled robust muscle survival and regeneration following significant cellular distress both in vitro and in vivo. By providing a biomimetic milieu to model muscle injury and repair, the described co-culture system could serve as a screening system to identify new pro-regenerative factors targeting muscle–macrophage interactions. Of significant interest, BMDMs within the injured muscle constructs exerted an anti-inflammatory, pro-regenerative response to on-site tissue damage resembling the actions of a cell pool not naturally prominent in native adult muscle: tissue-resident macrophages[67,68]. Further characterization of epigenetic changes in immune cells residing long-term within 3D engineered muscle milieu might allow the identification of mechanisms leading to the acquisition of specialized, pro-regenerative cell phenotypes[69]. Regarding the established roles of macrophages in the repair and vascularization of both muscle and various non-muscle tissues[7,70–72], our approach might inspire a broader use of immune system cells as the pro-regenerative constituent of transplanted tissue grafts. Lastly, our preliminary work with human blood-derived macrophages suggests similar anti-apoptotic and pro-regenerative roles of human immune system cells within this system, laying a foundation for the future development of patient-specific models.

Methods

Myogenic cell preparation.

Skeletal muscle tissue was isolated from the lower hind limbs of female adult Sprague–Dawley rats (~15 wk old) using the method described previously[16]. Specifically, tissues from the biceps femoris and vastus lateralis were extracted and washed twice in Wyles solution (Supplementary Table 1). All visible tendons and fat were removed and the remaining tissue was minced into a fine slurry in a 1.5 mg ml^{-1} collagenase digestion solution (Worthington). The digestion solution was passed through a 25 ml pipette at 1 and 1.5 h, at which point visible tendon and fat pieces were again removed from the solution using sterile forceps. At 2 h, the digestion solution was passed through a 10 ml pipette and the remaining non-digested tissue was removed. The remaining solution was passed through a 100 μ m cell strainer, spun down for 12 min at 400 r.c.f., resuspended in Wyles solution, passed through a 40 μ m cell strainer and again spun down. Cells were resuspended in Blau media (Supplementary Table 1) and pre-plated for 1 h before being supplemented with 5 ng ml^{-1} bFGF (PeproTech) and plated on Matrigel-coated plates. Myogenic cells used for in vitro regeneration assay and implantation studies were transduced by a lentivirus in which GCaMP6 expression was driven by a MHCK7 promoter for 24 h following initial cell seeding. Adult myogenic cells were expanded for 2–5 passages before engineered muscle

formation in which the cells were detached by the application of 2% dispase (*v/v*). Expanded cells were quantified for the presence of myogenic cells ($Pax7^+$, $MyoD^+$, $Ki67^+$ and $MyoG^+$) (Supplementary Table 2).

Neonatal skeletal muscle tissue was isolated from the lower hind limbs of P2 neonatal Sprague–Dawley rats. Tissue was extracted and washed twice in Wyles solution (Supplementary Table 1), then minced into a fine slurry and incubated in 1 mg ml^{-1} collagenase digestion solution at 37 °C (Worthington). The digestion solution was passed through a 10 ml pipette at 1.5 h. At 2 h, the digestion solution was passed again through a 10 ml pipette, and then through a 40 μm cell strainer. The strained solution was spun down and the cells were resuspended in Blau media (Supplementary Table 1) supplemented with 5 ng ml^{-1} bFGF (PeproTech) and plated on Matrigel-coated plates. Neonatal myogenic cells were expanded for 24 h, then detached by the application of 2% dispase (*v/v*) for engineered muscle formation.

BMDM isolation, differentiation and polarization.

BMDMs were derived from the in vitro differentiated bone marrow monocytes using methods adapted from published mouse protocols[73–75]. Specifically, following the removal of the hind limb muscle used for myogenic cell isolation, each lower leg was cleared of surrounding tissue, sectioned above the knee and washed twice in 70% ethanol and once in phosphate buffered saline (PBS), before two cuts were made in the tibia at the knee and at the junction of the fibula. The cuts exposed the bone marrow, which was flushed out with BMDM media (Supplementary Table 1) using a 20 gauge needle. Following disassociation of the marrow, it was strained and plated onto non-tissue culture plastic petri dishes at a density of 1 leg per 150 cm^2. BMDMs were cultured for 7–10 d in BMDM media to allow differentiation, with additional media being added at day 3. Differentiation of adherent cells was confirmed through staining with the macrophage-specific antibody CD68, as well as CD206 and inducible nitric oxide synthase to define the phenotype. After 7–10 d in culture, differentiated BMDMs were washed twice in warm PBS and dissociated with 0.05% trypsin before mixing with myogenic cells and the making of co-cultured engineered constructs.

Critical for macrophage phenotype and survival is M-CSF, which drives the differentiation of monocytes towards a macrophage phenotype[76]. M-CSF was derived from L929 cell-conditioned media (LCCM) and added to BMDM media and engineered muscle media at 30%. LCCM was generated by extracting conditioned media following 5–7 d of confluent L929 cell culture in a basal medium of high-glucose Dulbecco's modified Eagle's medium (DMEM) with 10% foetal bovine serum (FBS). L929 cells were gifted to us by the Chilkoti group, which previously reported a characteristic response of the cells to cytolysis by TNFα at picomolar concentrations[77,78] in a cell viability assay[79]. The cells were not specifically tested for mycoplasma contamination; however, there was no evidence of cell death with long-term culture.

To create positive controls for the immunostaining of markers of pro- and anti-inflammatory phenotypes, BMDMs were polarized using specific soluble factors. Rat recombinant IFNγ (50 ng ml^{-1}; R&D Systems) and lipopolysaccharide (100 ng ml^{-1}; Sigma–Aldrich) were

used to induce M1 polarization, and IL-10 (10 ng ml^{-1}; R&D Systems) was used to induce M2 polarization[74,80]. Factors were applied at day 7 of culture and left for 48 h.

BMDMSC isolation and differentiation.

Isolation of bone BMDMSCs was performed using similar methods to those described above for BMDMs. However, bone marrow cells, on removal, were subjected to a low-glucose DMEM medium with 10% FBS and seeded onto tissue culture plastic as described in the literature[29]. Similar to BMDMs, BMDMSCs were washed twice in warm PBS and dissociated with 0.05% trypsin before being used in engineered muscle.

Engineered muscle formation and culture.

All engineered muscle constructs were generated in two-construct polydimethylsiloxane (PDMS) moulds (7 mm long, 2 mm in diameter) cast from 3D-machined Teflon masters. PDMS moulds were sterilized in 70% ethanol and coated with 0.2% (*w/v*) pluronic (Invitrogen) to prevent hydrogel adhesion. Laser-cut porous, nylon (Cerex) frames were sterilized in 70% ethanol, completely dried and placed within the moulds to provide attachment for the hydrogel. The cell/hydrogel mixture—a fibrinogen-based gel consisting of Matrigel (Supplementary Table 1)—was injected into the PDMS wells, polymerized at 37 °C for 45 min and cultured on a rocker at 37 °C. Engineered muscle constructs were cultured under dynamic conditions at a ±30 ° tilt and 0.4 Hz[16,17,81]. Frames with constructs were removed from the moulds 2 d following construct formation and left to free-float in media thereafter. For the co-cultured constructs, BMDMs or BMDMSCs were added to the myogenic population at a ratio of 1:6. For the paracrine studies, one construct in a well contained both muscle cells and BMDMs (Mu–BMDM (referred to as P-Mu–BMDM for the paracrine studies)) and the other contained just muscle cells (Mu-only (referred to as P-Mu-only for the paracrine studies)). Growth medium (Supplementary Table 1) was used as the culture media for the first 4 d of culture and replaced by differentiation medium (Supplementary Table 1) to promote further fusion and differentiation of the myogenic cells. Degradation of fibrin was inhibited by 1 mg ml^{-1} aminocaproic acid (Sigma–Aldrich), LCCM was supplemented to all culture media at 30%, and 66% of the media was replaced each day. Cell-mediated hydrogel compaction generated passive tension, resulting in uniaxial cell alignment within the engineered muscle[82].

Real-time in vitro regeneration assay.

To track functional regeneration in live constructs, myogenic cells were transduced with MHCK7-GCaMP6 virus before construct formation, as described above. At day 10 of culture, constructs were injured by applying 0.4 μ M CTX. To induce mild and severe injury, bundles were exposed to CTX for 3 ±0.5 h and 6 ±0.5 h until a drop in the gCaMP6 signal to 25 or 50% of pre-injury values was achieved, respectively. Once the level of injury was achieved, the injured bundles were washed twice in DMEM and once in Differentiation Media for 15 min on the rocker. Functional and histological assessments were performed at 5, 10 and 15 d post-CTX along with measurements of cross-sectional myofibre area, cell proliferation and apoptosis. Every 2–3 d of culture, GCaMP6-reported calcium (Ca^{2+}) transients in electrically stimulated muscle constructs were imaged under sterile conditions. Constructs were transferred into a sterile electrical stimulation chamber containing stainless

steel field electrodes containing Tyrode's solution (Supplementary Table 1) and pinned to prevent motion artefacts. The chamber was then transferred to a temperaturecontrolled live imaging system and imaged with an Andor camera attached to a Nikon microscope. The muscle constructs were exposed to a train of stimuli (10 ms duration, 1 Hz, 90 V) and each construct was recorded for 2 s to capture at least one calcium transient. A MATLAB script was created to recognize the construct area in the stimulation movies and calculate the relative fluorescence intensity ($\Delta F/F$), as described previously[16]. Dependent on the experiment (severe versus mild), injury of a construct was induced by exposing it to CTX until 75% (~5–7 h) or 50% (~2–4 h) of $\Delta F/F$ was lost.

Cellular proliferation assay.

To track cumulative cell proliferation in muscle constructs, the modified thymidine analogue EdU (10 μM) was supplemented every day into the media following CTX injury. The EdU kit (Thermo Fisher Scientific) includes a fluorophore capable of detecting the EdU once it has incorporated into newly synthesized DNA.

Supplementation of pro-regenerative and anti-apoptotic factors and proinflammatory inhibitors.

Rat recombinant proteins were supplemented every day to engineered muscle at their working concentrations: IGF-1 (20 ng ml^{-1}; R&D Systems), IL-10 (20 ng ml^{-1}; R&D Systems) and G-CSF (20 ng ml^{-1}; PeproTech). The anti-apoptotic factor Q-VD-OPh (2.5 μM; Sigma–Aldrich), a pancaspase inhibitor, was supplemented daily up to 10 d after CTX injury. Small molecule inhibitors of TNFα —SPD304 (ref. [50]) (5 and 10 μM; Sigma–Aldrich) and C87 (ref.[83]) (5 μM; Tocris)—were supplemented daily up to 15 d after CTX injury. All factors were added to the media immediately after CTX injury.

Immunostaining.

Engineered muscle constructs were fixed in 2% formaldehyde (Electron Microscopy Sciences) overnight on a rocker at 4 °C. Samples were treated using a blocking solution (0.5% Triton-X and 5% chicken serum PBS) overnight on a rocker at 4 °C. Primary antibody solutions (Supplementary Table 2) at 1:15–1:300 dilution were applied in blocking solution overnight on a rocker at 4 °C. Samples were then washed 3 times in 0.1% Triton-X and incubated in secondary antibody (1:200 dilution in blocking solution; Life Technologies) with 4′, 6-diamidino-2-phenylindole (DAPI) and/or Alexa Fluor 488-conjugated phalloidin (Invitrogen) overnight on a rocker at 4 °C. Fluorescence images were acquired on an inverted confocal microscope (Zeiss LSM 510) at 10–40× magnification. Constructs were sectioned parallel (longitudinal) and perpendicular (transverse) to the long axis. Samples were submerged in optimal cutting temperature compound (Electron Microscopy Sciences), snap-frozen in liquid nitrogen, sliced (12 μm thick) and mounted on glass slides, followed by blocking and application of the antibodies. Specific primary antibodies are presented in Supplementary Table 2. TUNEL labelling to visualize the occurrence of apoptotic cell death within engineered muscle following injury was performed using a commercially available kit (Thermo Fisher Scientific) in both longitudinal and transverse sections.

For quantitative analyses of nuclear stains, we utilized a custom ImageJ (Fiji) programme that identifies areas stained for DAPI, transcription factor (Pax7, MyoD or MyoG) or proliferation marker (Ki67) and, based on the median nucleus size for a given magnification, designates and automatically counts the identified nuclei as described previously[16].

In our analysis, when discrete stains (nuclear markers; for example, Pax7 or MyoD) or labelling of cell types (for example, $CD206^+$ macrophages) were clearly visible, events were counted individually. If expression could not be directly assigned to individual cells (for example, cleaved caspase-3 staining), the average area per nuclear count was expressed.

Quantitative cytokine analysis.

Conditioned media was collected from Mu-only and Mu–BMDM tissues during the in vitro regeneration assay pre-injury and at days 2, 5, 10 and 15 post-injury. Consistent with previous experiments, all tissues were exposed to culture media containing 30% LCCM, and 66% of the media was replaced each day. Specific cytokine concentrations were measured using a Quantibody Array Kit following the manufacturer's instructions (RayBiotech).

Implantation of adult-derived engineered muscle constructs.

All animal experiments were approved by the Duke University Institutional Animal Care and Use Committee and were in compliance with ethical regulations. Sample sizes were determined based on previous use of the implantation method[16]. Before surgery, athymic nude mice (~10 weeks of age; 22–30 g; assorted sexes) were anaesthetized by intraperitoneal injection of ketamine (100 mg kg^{-1}) and xylazine (10 mg kg^{-1}). Surgical techniques associated with the dorsal window-chamber implantation were performed as previously reported[16]. Specifically, using the aseptic technique, the dorsal skin was attached to a temporary 'C-frame' at the centre of the back. The skin was perforated in three locations to accommodate the screws of the chamber, and a circular region (~12 mm) of the forward-facing skin (that is, the cutis, subcutis, retractor and panniculus carnosis muscles, and associated fascia) was dissected away to accommodate the window proper. The forward and rearward pieces of the titanium dorsal skinfold chamber were assembled together from opposite sides of the skin, and a muscle construct was laid perpendicular (verified under microscope) to the intact panniculus carnosis muscle of the rearward-facing skin, providing a source of microvessels for vascularization. A sterile cover glass was placed over the window and engineered tissue while superfusing with sterile saline solution. The chamber was then secured with sutures and the 'C-frame' was removed. Postoperatively, mice were injected subcutaneously with buprenorphine (1 mg kg^{-1}) painkiller and left to recover on a heating pad. The surgeon was blinded from the experimental group during surgery and the order was randomly selected beforehand.

Intravital imaging of blood vessels and intracellular Ca^{2+} transients.

Intravital recordings were performed in anaesthetized mice on days 2, 5, 7, 9, 12 and 15 post-implantation. Mice were anaesthetized by nose cone inhalation of isoflurane and positioned on a heating pad under a microscope objective. Hyperspectral brightfield image sequences (10 nm increments from 500–600 nm) were captured at 5× magnification using a tunable filter (Cambridge Research & Instrumentation) and a digital video camera

(Thorlabs), as previously described[16,84]. A custom MATLAB (MathWorks) script[85] was applied to create maps of the total haemoglobin concentration. Obtained maps were further processed using local contrast enhancement in ImageJ (Fiji) and thresholded to binary images to identify the vessel area and calculate the blood vessel density (total area of blood vessels per construct area) as described previously[16]. Intravital imaging of spontaneous Ca^{2+} transients was performed immediately after vessel imaging with mice still anaesthetized. Fluorescent GCaMP6 signals in implanted constructs were videoimaged through a fluorescein isothiocyanate filter using a fast fluorescent camera (Andor) at 16 μm spatial resolution and 20 ms temporal resolution. Amplitudes of spontaneous Ca^{2+} transients were calculated using a custom MATLAB (MathWorks) script averaging $\Delta F/F$ of 25 μm ×25 μm regions spanning the area of the implanted construct.

In vitro and ex vivo force measurements.

Engineered muscle constructs were loaded into a custom-made force measurement set-up containing a sensitive optical force transducer and a linear actuator (Thorlabs), as previously described[82]. Samples were stimulated (10 ms, 3 V mm^{-1} pulses) at different frequencies (single pulse to 40 Hz), and isometric active (contractile) forces were measured at different muscle lengths. The specific force was calculated by dividing the active force by the cross-sectional muscle area.

Ex vivo calcium measurements.

Electrically induced Ca^{2+} transient amplitudes, reported as $\Delta F/F$[16], were measured in explanted constructs at days 5, 10 and 15 post-implantation using the live cell chamber described above. Twitch (1 10 ms pulse, 1 Hz, 3 V mm^{-1}) and tetanic (40 10 ms pulses, 40 Hz, 3 V mm^{-1}) contractions were assessed.

Human blood monocyte-derived macrophage isolation

he below procedure was adapted from a protocol shared with us by B. Chazaud. Human umbilical cord blood was obtained from the Carolinas Cord Blood Bank using a protocol (Pro00013890) approved by the Duke University Health System Institutional Review Board and diluted 1:1 with PBS. To isolate the buffy coat, 30 ml of the diluted blood was layered over 18 ml of Lymphoprep or Histopaque (at a density of 1.077 g ml^{-1}) and spun at 1,800 *g* for 30 min with no brake. Following centrifugation, the buffy coat was collected and diluted 1:3 with PBS. The diluted buffy coat was spun down at 450 *g* for 7 min. The supernatant was then removed and 20 ml of red blood cell lysis buffer (BD Pharmingen) was added to the pellet. The buffer/cell solution was placed on a shaker for 10 min and vortexed at the 5 and 10 min time points. Next, the solution was spun at 450 *g* for 7 min and assessed to see whether the pellet was red in colour, indicating remaining red blood cells. If the pellet was white, it was resuspended in PBS to wash. If not, the lysis step was repeated using half the original volume. From the remaining cells, $CD14^+$ monocytes were purified via magnetic-activated cell sorting (MACS; Miltenyi Biotec) using human CD14 microbeads (Miltenyi Biotec). The positive cell fraction was spun at 450 *g* for 7 min, resuspended in RPMI 1640 (10% heat inactivated FBS and 50 ng ml^{-1} human M-CSF (PeproTech)) at 400,000 cells ml^{-1} and plated at 25,000 cells cm^{-2}. On day 5, the media was completely changed. From day 6 to 21, the differentiated human macrophages were added to skeletal muscle cells as

described above to engineer hybrid muscle–macrophage tissues. A human-specific CD68 antibody was used to confirm the species of the cells (Supplementary Fig. 17a).

Quantitative PCR.

Total RNA was isolated according to the RNeasy Fibrous Tissue Mini Kit (Qiagen) and the concentration was measured using a NanoDrop 1000. Depending on the experiment group and time point post-injury, RNA was pooled between 2 and 6 constructs (BMDM-only and Mu-only constructs at late time points required more samples). Reverse transcription was run on equal amounts of RNA using an iScript cDNA Synthesis Kit (Bio-Rad). Quantitative PCR was performed using an iTaq Universal SYBR Green Supermix kit (Bio-Rad). The relative expression of indicated genes was quantified by the ΔΔ CT method, using β −2 microglobulin (B2M) as the housekeeping gene. Primer sequences are listed in Supplementary Table 3.

Statistics.

Unless specified, the results are presented as means ±s.e.m. Statistical significances among different groups were evaluated with the tests described in the figure captions using GraphPad Prism (GraphPad Software). $P<0.05$ was considered statistically significant. Different levels of significance are noted in the figures and figure captions. Supplementary Table 4 lists the exact P values where they are greater than 0.0001. There was no estimation of variation, and the variance was similar between all groups being statistically compared. Sample sizes were determined based on the variance of previously reported measurements[16,17]. All shown immunostainings and videos are representative of similar results obtained from at least three independent experiments.

Supplementary Material

Refer to Web version on PubMed Central for supplementary material.

Acknowledgements

We acknowledge C. Jackman, A. Khodabukus, L. Li, I. Shadrin, A. Ganapathi, G. Palmer and G. Hanna for technical assistance, and the Light Microscopy and Optical Molecular Imaging and Analysis core facilities at Duke University for use of their resources. We also thank B. Chazaud for granting a protocol for human macrophage derivation. This study was supported by the National Science Foundation's Graduate Research Fellowship to M.J., and grants AR070543 and AR065873 from the National Institute of Arthritis and Musculoskeletal and Skin Diseases to N.B.

References

1. Charge SB & Rudnicki MA Cellular and molecular regulation of muscle regeneration. Physiol. Rev 84, 209–238 (2004). [PubMed: 14715915]
2. Lepper C, Partridge TA & Fan CM An absolute requirement for Pax7-positive satellite cells in acute injury-induced skeletal muscle regeneration. Development 138, 3639–3646 (2011). [PubMed: 21828092]
3. Yin H, Price F & Rudnicki MA Satellite cells and the muscle stem cell niche. Physiol. Rev93, 23–67 (2013). [PubMed: 23303905]

4. Tidball JG & Villalta SA Regulatory interactions between muscle and the immune system during muscle regeneration. Am. J. Physiol. Regul. Integr. Comp. Physiol 298, R1173–R1187 (2010). [PubMed: 20219869]
5. Kharraz Y, Guerra J, Mann CJ, Serrano AL & Munoz-Canoves P Macrophage plasticity and the role of inflammation in skeletal muscle repair. Mediators Inflamm. 2013, 491497 (2013). [PubMed: 23509419]
6. Saclier M et al. Differentially activated macrophages orchestrate myogenic precursor cell fate during human skeletal muscle regeneration. Stem Cells 31, 384–396 (2013). [PubMed: 23169615]
7. Tidball JG, Dorshkind K & Wehling-Henricks M Shared signaling systems in myeloid cell-mediated muscle regeneration. Development 141, 1184–1196 (2014). [PubMed: 24595286]
8. Turner NJ & Badylak SF Regeneration of skeletal muscle. Cell Tissue Res. 347, 759–774 (2012). [PubMed: 21667167]
9. Blau HM, Cosgrove BD & Ho AT The central role of muscle stem cells in regenerative failure with aging. Nat. Med. 21, 854–862 (2015). [PubMed: 26248268]
10. Sacco A et al. Short telomeres and stem cell exhaustion model Duchenne muscular dystrophy in mdx/mTR mice. Cell 143, 1059–1071 (2010). [PubMed: 21145579]
11. Bhatia SN & Ingber DE Microfluidic organs-on-chips. Nat. Biotechnol 32, 760–772 (2014). [PubMed: 25093883]
12. Clevers H Modeling development and disease with organoids. Cell 165, 1586–1597 (2016). [PubMed: 27315476]
13. Quarta M et al. An artificial niche preserves the quiescence of muscle stem cells and enhances their therapeutic efficacy. Nat. Biotechnol 34, 752–759 (2016). [PubMed: 27240197]
14. Cosgrove BD et al. Rejuvenation of the muscle stem cell population restores strength to injured aged muscles. Nat. Med 20, 255–264 (2014). [PubMed: 24531378]
15. Gilbert PM et al. Substrate elasticity regulates skeletal muscle stem cell self-renewal in culture. Science 329, 1078–1081 (2010). [PubMed: 20647425]
16. Juhas M, Engelmayr GC Fontanella AN, Jr, Palmer GM & Bursac N Biomimetic engineered muscle with capacity for vascular integration and functional maturation in vivo. Proc. Natl Acad. Sci. USA 111, 5508–5513 (2014). [PubMed: 24706792]
17. Juhas M & Bursac N Roles of adherent myogenic cells and dynamic culture in engineered muscle function and maintenance of satellite cells. Biomaterials 35, 9438–9446 (2014). [PubMed: 25154662]
18. Close R Dynamic properties of fast and slow skeletal muscles of rat during development. J. Physiol. 173, 74–95 (1964). [PubMed: 14205033]
19. Chen TW et al. Ultrasensitive fluorescent proteins for imaging neuronal activity. Nature 499, 295–300 (2013). [PubMed: 23868258]
20. Madden L, Juhas M, Kraus WE, Truskey GA & Bursac N Bioengineered human myobundles mimic clinical responses of skeletal muscle to drugs. eLife 4, e04885 (2015). [PubMed: 25575180]
21. Salva MZ et al. Design of tissue-specific regulatory cassettes for high-level rAAV-mediated expression in skeletal and cardiac muscle. Mol. Ther 15, 320–329 (2007). [PubMed: 17235310]
22. Pelosi L et al. Local expression of IGF-1 accelerates muscle regeneration by rapidly modulating inflammatory cytokines and chemokines. FASEB J 21, 1393–1402 (2007). [PubMed: 17264161]
23. Deng B, Wehling-Henricks M, Villalta SA, Wang Y & Tidball JG IL-10 triggers changes in macrophage phenotype that promote muscle growth and regeneration. J. Immunol 189, 3669–3680 (2012). [PubMed: 22933625]
24. Hayashiji N et al. G-CSF supports long-term muscle regeneration in mouse models of muscular dystrophy. Nat. Commun 6, 6745 (2015). [PubMed: 25865621]
25. Schleicher U & Bogdan C Generation, culture and flow-cytometric characterization of primary mouse macrophages. Methods Mol. Biol 531, 203–224 (2009). [PubMed: 19347320]
26. Hamilton JA Colony-stimulating factors in inflammation and autoimmunity. Nat. Rev. Immunol 8, 533–544 (2008). [PubMed: 18551128]
27. Fleetwood AJ, Lawrence T, Hamilton JA & Cook AD Granulocyte-macrophage colony-stimulating factor (CSF) and macrophage CSF-dependent macrophage phenotypes display differences in

cytokine profiles and transcription factor activities: implications for CSF blockade in inflammation. J. Immunol 178, 5245–5252 (2007). [PubMed: 17404308]

28. Krause MP et al. Impaired macrophage and satellite cell infiltration occurs in a muscle-specific fashion following injury in diabetic skeletal muscle. PLoS ONE 8, e70971 (2013). [PubMed: 23951058]
29. Soleimani M & Nadri S A protocol for isolation and culture of mesenchymal stem cells from mouse bone marrow. Nat. Protoc 4, 102–106 (2009). [PubMed: 19131962]
30. Dirks A & Leeuwenburgh C Apoptosis in skeletal muscle with aging. Am. J. Physiol. Regul. Integr. Comp. Physiol 282, R519–R527 (2002). [PubMed: 11792662]
31. Stratos I et al. Inhibition of caspase mediated apoptosis restores muscle function after crush injury in rat skeletal muscle. Apoptosis 17, 269–277 (2012). [PubMed: 22089165]
32. Wang H et al. Turning terminally differentiated skeletal muscle cells into regenerative progenitors. Nat. Commun. 6, 7916 (2015). [PubMed: 26243583]
33. Fernando P, Kelly JF, Balazsi K, Slack RS & Megeney LA Caspase 3 activity is required for skeletal muscle differentiation. Proc. Natl Acad. Sci. USA 99, 11025–11030 (2002). [PubMed: 12177420]
34. Chazaud B et al. Satellite cells attract monocytes and use macrophages as a support to escape apoptosis and enhance muscle growth. J. Cell. Biol 163, 1133–1143 (2003). [PubMed: 14662751]
35. Sonnet C et al. Human macrophages rescue myoblasts and myotubes from apoptosis through a set of adhesion molecular systems. J. Cell. Sci 119, 2497–2507 (2006). [PubMed: 16720640]
36. Kondo M et al. Roles of proinflammatory cytokines and the Fas/Fas ligand interaction in the pathogenesis of inflammatory myopathies. Immunology 128, e589–e599 (2009). [PubMed: 19740320]
37. Kalovidouris AE & Plotkin Z Synergistic cytotoxic effect of interferon-gamma and tumor necrosis factor-alpha on cultured human muscle cells. J. Rheumatol 22, 1698–1703 (1995). [PubMed: 8523348]
38. Reid MB & Li YP Tumor necrosis factor-alpha and muscle wasting: a cellular perspective. Respir. Res 2, 269–272 (2001). [PubMed: 11686894]
39. Pistilli EE, Jackson JR & Alway SE Death receptor-associated pro-apoptotic signaling in aged skeletal muscle. Apoptosis 11, 2115–2126 (2006). [PubMed: 17051337]
40. Geng YJ, Wu Q, Muszynski M, Hansson GK & Libby P Apoptosis of vascular smooth muscle cells induced by in vitro stimulation with interferongamma, tumor necrosis factor-alpha, and interleukin-1 beta. Arterioscler. Thromb. Vasc. Biol 16, 19–27 (1996). [PubMed: 8548421]
41. Pedersen BK Exercise-induced myokines and their role in chronic diseases. Brain Behav. Immun 25, 811–816 (2011). [PubMed: 21354469]
42. Pedersen BK, Steensberg A & Schjerling P Muscle-derived interleukin-6: possible biological effects. J. Physiol 536, 329–337 (2001). [PubMed: 11600669]
43. Rehman J et al. Dynamic exercise leads to an increase in circulating ICAM-1: further evidence for adrenergic modulation of cell adhesion. Brain Behav. Immun 11, 343–351 (1997). [PubMed: 9512820]
44. Villalta SA et al. Interleukin-10 reduces the pathology of mdx muscular dystrophy by deactivating M1 macrophages and modulating macrophage phenotype. Hum. Mol. Genet 20, 790–805 (2011). [PubMed: 21118895]
45. Zeng L et al. Insulin-like 6 is induced by muscle injury and functions as a regenerative factor. J. Biol. Chem. 285, 36060–36069 (2010). [PubMed: 20807758]
46. Munoz-Canoves P, Scheele C, Pedersen BK & Serrano AL Interleukin-6 myokine signaling in skeletal muscle: a double-edged sword? FEBS J. 280, 4131–4148 (2013). [PubMed: 23663276]
47. Jablonski KA et al. Novel markers to delineate murine M1 and M2 macrophages. PLoS ONE 10, e0145342 (2015). [PubMed: 26699615]
48. Wajant H, Pfizenmaier K & Scheurich P Tumor necrosis factor signaling. Cell Death Differ. 10, 45–65 (2003). [PubMed: 12655295]
49. Grounds MD & Torrisi J Anti-TNFalpha (Remicade) therapy protects dystrophic skeletal muscle from necrosis. FASEB J. 18, 676–682 (2004). [PubMed: 15054089]

50. He MM et al. Small-molecule inhibition of TNF-alpha. Science 310, 1022–1025 (2005). [PubMed: 16284179]
51. Chen SE et al. Role of TNF-α signaling in regeneration of cardiotoxininjured muscle. Am. J. Physiol. Cell Physiol 289, C1179–C1187 (2005). [PubMed: 16079187]
52. Cheng M, Nguyen MH, Fantuzzi G & Koh TJ Endogenous interferon-gamma is required for efficient skeletal muscle regeneration. Am. J. Physiol. Cell Physiol 294, C1183–C1191 (2008). [PubMed: 18353892]
53. Montarras D et al. Direct isolation of satellite cells for skeletal muscle regeneration. Science 309, 2064–2067 (2005). [PubMed: 16141372]
54. Day K, Shefer G, Shearer A & Yablonka-Reuveni Z The depletion of skeletal muscle satellite cells with age is concomitant with reduced capacity of single progenitors to produce reserve progeny. Dev. Biol. 340, 330–343 (2010). [PubMed: 20079729]
55. Tierney MT et al. Autonomous extracellular matrix remodeling controls a progressive adaptation in muscle stem cell regenerative capacity during development. Cell Rep. 14, 1940–1952 (2016). [PubMed: 26904948]
56. Lees SJ, Zwetsloot KA & Booth FW Muscle precursor cells isolated from aged rats exhibit an increased tumor necrosis factor-alpha response. Aging Cell 8, 26–35 (2009). [PubMed: 19053972]
57. Fulle S, Sancilio S, Mancinelli R, Gatta V & Di Pietro R Dual role of the caspase enzymes in satellite cells from aged and young subjects. Cell Death Dis. 4, e955 (2013). [PubMed: 24336075]
58. Davis TA & Fiorotto ML Regulation of muscle growth in neonates. Curr. Opin. Clin. Nutr 12, 78–85 (2009).
59. Dogra C, Changotra H, Mohan S & Kumar A Tumor necrosis factor-like weak inducer of apoptosis inhibits skeletal myogenesis through sustained activation of nuclear factor-κB and degradation of MyoD protein. J. Biol. Chem 281, 10327–10336 (2006). [PubMed: 16461349]
60. Bruunsgaard H, Pedersen M & Pedersen BK Aging and proinflammatory cytokines. Curr. Opin. Hematol 8, 131–136 (2001). [PubMed: 11303144]
61. Collins RA & Grounds MD The role of tumor necrosis factor-α (TNF-α) in skeletal muscle regeneration. Studies in TNF-α −/− and TNF-α −/−/LT-α- /- mice. J. Histochem. Cytochem 49, 989–1001 (2001). [PubMed: 11457927]
62. Ochoa O et al. Delayed angiogenesis and VEGF production in CCR2$^{-/-}$ mice during impaired skeletal muscle regeneration. Am. J. Physiol. Regul. Integr. Comp. Physiol 293, R651–R661 (2007). [PubMed: 17522124]
63. Chung ES et al. Contribution of macrophages to angiogenesis induced by vascular endothelial growth factor receptor-3-specific ligands. Am. J. Pathol 175, 1984–1992 (2009). [PubMed: 19808642]
64. Nucera S, Biziato D & De Palma M The interplay between macrophages and angiogenesis in development, tissue injury and regeneration. Int. J. Dev. Biol 55, 495–503 (2011). [PubMed: 21732273]
65. Vignaud A et al. Impaired skeletal muscle repair after ischemia–reperfusion injury in mice. J. Biomed. Biotechnol 2010, 724914 (2010). [PubMed: 20467471]
66. Lee SL, Pevec WC & Carlsen RC Functional outcome of new blood vessel growth into ischemic skeletal muscle. J. Vasc. Surg 34, 1096–1102 (2001). [PubMed: 11743567]
67. Davies LC, Jenkins SJ, Allen JE & Taylor PR Tissue-resident macrophages. Nat. Immunol 14, 986–995 (2013). [PubMed: 24048120]
68. Mantovani A, Biswas SK, Galdiero MR, Sica A & Locati M Macrophage plasticity and polarization in tissue repair and remodelling. J. Pathol 229, 176–185 (2013). [PubMed: 23096265]
69. Lavin Y et al. Tissue-resident macrophage enhancer landscapes are shaped by the local microenvironment. Cell 159, 1312–1326 (2014). [PubMed: 25480296]
70. Das A et al. Monocyte and macrophage plasticity in tissue repair and regeneration. Am. J. Pathol 185, 2596–2606 (2015). [PubMed: 26118749]
71. Forbes SJ & Rosenthal N Preparing the ground for tissue regeneration: from mechanism to therapy. Nat. Med 20, 857–869 (2014). [PubMed: 25100531]

72. Aurora AB et al. Macrophages are required for neonatal heart regeneration. J. Clin. Invest. 124, 1382–1392 (2014). [PubMed: 24569380]

73. Kanters E et al. Hematopoietic NF-kappaB1 deficiency results in small atherosclerotic lesions with an inflammatory phenotype. Blood 103, 934–940 (2004). [PubMed: 14512319]

74. Lesault PF et al. Macrophages improve survival, proliferation and migration of engrafted myogenic precursor cells into MDX skeletal muscle. PLoS ONE 7, e46698 (2012). [PubMed: 23056408]

75. Stanley ER Murine bone marrow-derived macrophages. Methods Mol. Biol 75, 301–304 (1997). [PubMed: 9276279]

76. Gleissner CA, Shaked I, Little KM & Ley K CXC chemokine ligand 4 induces a unique transcriptome in monocyte-derived macrophages. J. Immunol 184, 4810–4818 (2010). [PubMed: 20335529]

77. Flick DA & Gifford GE Comparison of in vitro cell cytotoxic assays for tumor necrosis factor. J. Immunol. Methods 68, 167–175 (1984). [PubMed: 6707477]

78. Liddil JD, Dorr RT & Scuderi P Association of lysosomal activity with sensitivity and resistance to tumor necrosis factor in murine L929 cells. Cancer Res. 49, 2722–2728 (1989). [PubMed: 2713856]

79. Bellucci JJ, Amiram M, Bhattacharyya J, McCafferty D & Chilkoti A Three-in-one chromatography-free purification, tag removal, and site-specific modification of recombinant fusion proteins using sortase A and elastin-like polypeptides. Angew. Chem. Int. Ed. Engl 52, 3703–3708 (2013). [PubMed: 23424160]

80. Jetten N et al. Anti-inflammatory M2, but not pro-inflammatory M1 macrophages promote angiogenesis in vivo. Angiogenesis 17, 109–118 (2014). [PubMed: 24013945]

81. Jackman CP, Carlson AL & Bursac N Dynamic culture yields engineered myocardium with near-adult functional output. Biomaterials. 111, 66–79 (2016). [PubMed: 27723557]

82. Hinds S, Bian W, Dennis RG & Bursac N The role of extracellular matrix composition in structure and function of bioengineered skeletal muscle. Biomaterials 32, 3575–3583 (2011). [PubMed: 21324402]

83. Ma L et al. A novel small-molecule tumor necrosis factor alpha inhibitor attenuates inflammation in a hepatitis mouse model. J. Biol. Chem 289, 12457–12466 (2014). [PubMed: 24634219]

84. Palmer GM et al. In vivo optical molecular imaging and analysis in mice using dorsal window chamber models applied to hypoxia, vasculature and fluorescent reporters. Nat. Protoc 6, 1355–1366 (2011). [PubMed: 21886101]

85. Palmer GM, Fontanella AN, Shan S & Dewhirst MW High-resolution in vivo imaging of fluorescent proteins using window chamber models. Methods Mol. Biol 872, 31–50 (2012). [PubMed: 22700402]

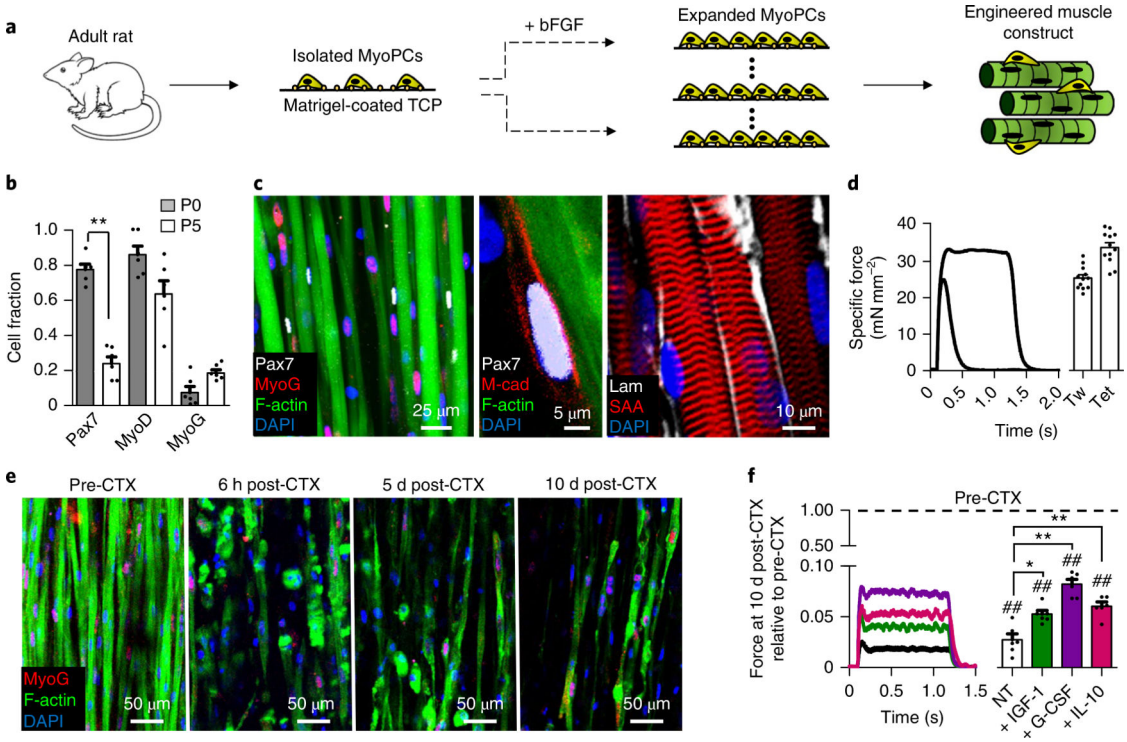

Fig. 1 |. Function and injury response of adult-rat-derived skeletal muscle constructs.

a, Schematic depicting the isolation and expansion of MyoPCs in bFGF-containing media on Matrigel-coated tissue culture plastic (TCP). After 3–5 passages, expanded MyoPCs were used to engineer 3D skeletal muscle tissues. **b**, Cell fractions positive for the myogenic markers Pax7, MyoD and MyoG in MyoPCs at passages 0 (P0) and 5 (P5) during expansion. $^{**}P < 0.001$ ($n = 6$ independent samples). **c**, Two-week cultured engineered muscle harbours a pool of M-cadherin (M-cad)+/Pax7+ MuSCs abutting cross-striated myofibres (labelled with sarcomeric α -actinin (SAA)) that contain MyoG+ myonuclei (left; the middle panel shows a magnified image of a myonucleus) and are enveloped in laminin (Lam)-rich matrix (right). **d**, Representative traces of twitch (Tw) and tetanus (Tet) contractile forces generated by engineered muscle in response to electrical stimulation (left) and quantified force amplitudes (right) ($n = 12$ independent experiments). **e**, Representative images of myofibres and MyoG+ myonuclei within (from left to right) engineered muscle pre-injury, and 6 h, 5 d and 10 d post-CTX administration. MyoG+ myonuclei are shown in red, F-actin in green and DAPI in blue. **f**, Representative tetanus traces (left) and quantified force amplitudes (right) at 10 d postCTX injury relative to pre-CTX levels in non-treated (NT) muscles (black) and those treated with the pro-regenerative factors IGF-1 (20 nM, green), G-CSF (10 nM, purple) and IL-10 (20 nM, red). $^{**}P < 0.001$ and $^{*}P < 0.05$ compared with NT at 10 d post-CTX; and $^{\#\#}P < 0.001$ compared with pre-CTX ($n = 6$ independent samples). All bars included within brackets are statistically different versus pre-CTX. The dashed line represents normalization to pre-CTX Mu-only. All bars denote means ± s.e.m. Significance was determined by a two-sided *t*-test in **b** and analysis of variance and Tukey's multiple comparison post-hoc tests in **f**. Supplementary Table 4 lists exact *P* values when greater than 0.0001.

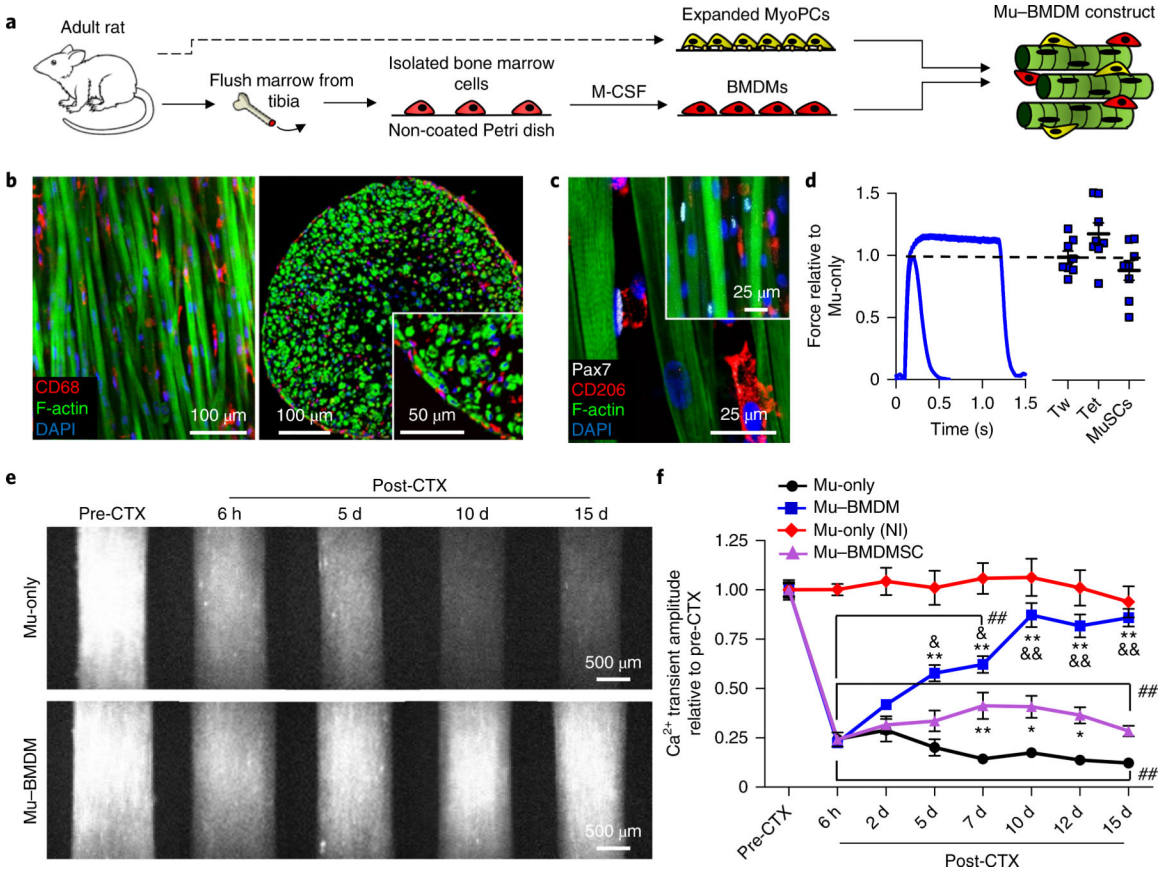

Fig. 2 |. Structure, function and Ca^{2}+ transient injury response of adult-derived Mu–BMdM constructs.

a, Schematic describing the engineering of Mu–BMDM tissues using a mixture of expanded MyoPCs and BMDMs obtained from the same adult rats. **b**,**c**, Representative images of Mu–BMDM constructs showing longitudinal (**b**, left) and transverse sections (**b**, right) of the distribution of CD68+ BMDMs (inset, higher-magnification image of BMDMs dispersed among myofibres labelled with F-actin), and Pax7+ MuSCs and CD206+ BMDMs in the longitudinal section (**c**) (inset, lowermagnification image of a Mu–BMDM construct). Pax7+ MuSCs are shown in white, CD68+/CD206+ BMDMs in red, F-actin in green and DAPI in blue. **d**, Representative force traces (left) and quantified twitch (Tw) and tetanus (Tet) force and MuSC density (right) in Mu–BMDM relative to Mu-only constructs ($n = 8$ independent samples). The dashed line represents normalization to Mu-only. **e**, Peak GCaMP6 fluorescence signals (from left to right) pre-CTX and 6 h, 5 d, 10 d and 15 d post-CTX-induced injury in adult-derived Mu-only (top) and Mu–BMDM constructs (bottom). **f**, Quantified signal amplitudes in injured Mu-only, Mu–BMDM and Mu–BMDMSC constructs, and Mu-only non-injured (NI) constructs. $^{*}P < 0.05$ and $^{**}P < 0.001$ compared with Mu-only; $^{\&}P < 0.05$ and $^{\&\&}P < 0.001$ compared with Mu–BMDMSC; and $^{\#\#}P < 0.001$ compared with NI Mu-only. The symbol dictating significance is designated to each point included within the brackets ($n = 20$ for Mu-only and Mu–BMDM; $n = 12$ for Mu–BMDMSC; and $n = 6$ independent samples for Mu-only (NI)). Significance was determined by two-way analysis of variance with post-hoc Bonferroni-corrected two-sided *t*-tests. All

bars and points denote means ± s.e.m. Supplementary Table 4 lists exact *P* values when greater than 0.0001.

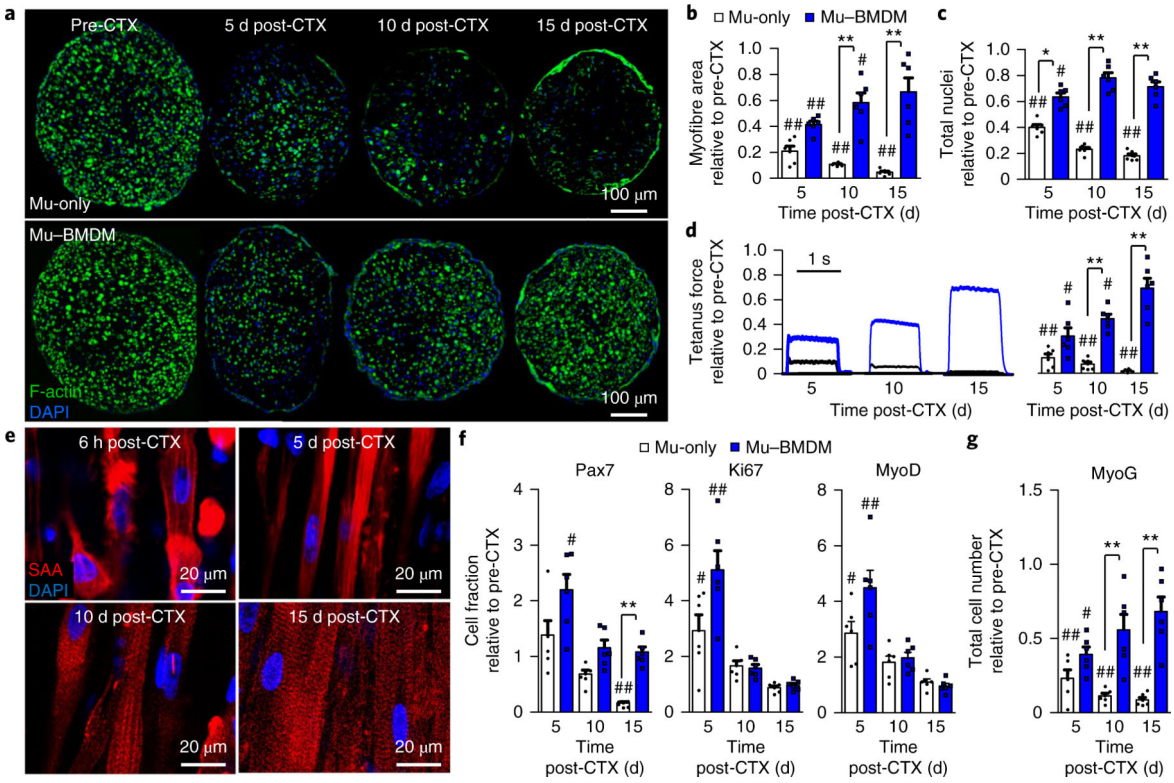

Fig. 3 |. Structural, functional and myogenic recovery from CTX-induced in vitro injury in Mu–BMdM constructs.

a, Transverse cross-sectional staining of Mu-only (top) and Mu–BMDM (bottom) constructs (from left to right) pre-CTX and at 5, 10 and 15 d post-CTX injury. Myofibres were labelled with F-actin (green). **b**,**c**, Quantified recovery of myofibre area (**b**) and total nuclei numbers (**c**) over 15 d post-injury relative to pre-CTX levels. **d**, Representative force traces (left) and quantified recovery (right) of tetanic force generation in Mu-only and Mu–BMDM constructs over 15 d post-CTX. In **b**–**d**, $*P < 0.05$, and $**P < 0.001$ for comparisons between groups; and $^{\#}P < 0.05$ and $^{\#\#}P < 0.001$ compared with pre-CTX levels ($n = 6$ independent experiments). **e**, Representative longitudinal sections showing sarcomeric reformation (labelled with sarcomeric α- actinin (SAA)) in Mu–BMDM constructs 6 h (top left), 5 d (top right), 10 d (bottom left) and 15 d (bottom right) after CTX injury. **f**,**g**, Plots of the fold-change in the fraction of Pax7+, Ki67+ and MyoD+ (**f**) and total MyoG+ cell numbers (**g**) at 5, 10 and 15 d post-CTX relative to pre-CTX levels. $**P < 0.001$. $^{\#}P < 0.05$, $^{\#\#}P < 0.001$ compared with pre-CTX levels ($n = 6$ independent samples). All bars denote means ± s.e.m. Significance was determined by two-way analysis of variance and post-hoc two-sided *t*-tests (relative to pre-CTX levels) in **d** or Tukey's multiple comparison post-hoc tests (between groups at specific time points) in **b**, **c**, **f** and **g**. Supplementary Table 4 lists exact *P* values when greater than 0.0001.

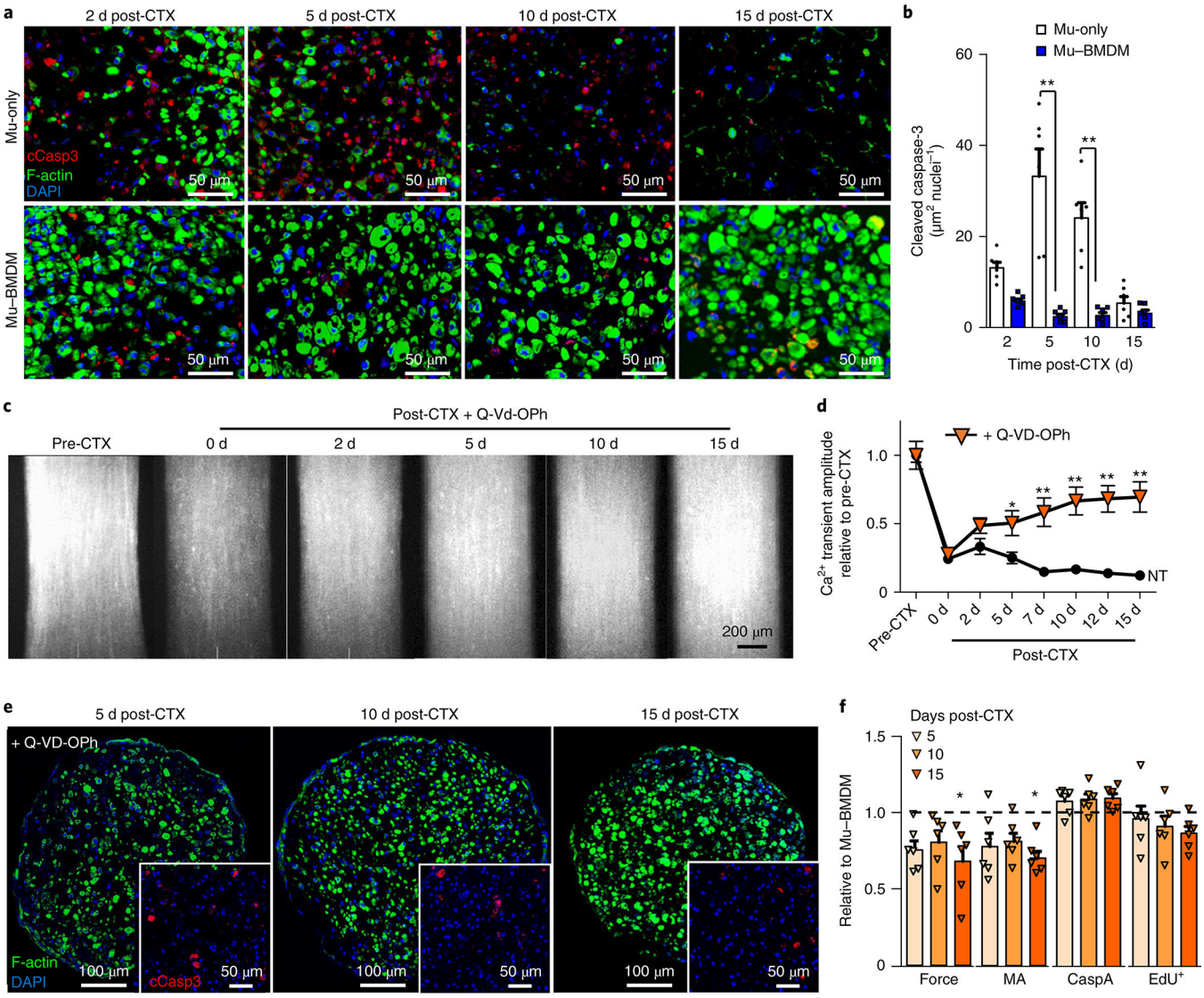

Fig. 4 |. Anti-apoptotic effect of BMdMs leads to enhanced regeneration in vitro.

a,**b**, Representative cross-sectional staining of cleaved caspase-3 (cCasp3) and myofibres (labelled with F-actin) (**a**) and quantified caspase-3 area over total nuclei (**b**) in Mu-only and Mu–BMDM constructs at days 2, 5, 10 and 15 post-injury. $^{**}P < 0.01$ ($n = 6$ independent experiments). **c**,**d**, Peak GCaMP6 signals in Mu-only constructs pre- and post-CTX injury supplemented with the pan-caspase inhibitor Q-VD-OPh (**c**), and quantified Ca^{2+} transient amplitude during 15 d post-injury with Q-Vd-OPh supplementation versus no treatment (NT) (**d**). $^{*}P < 0.05$ and $^{**}P < 0.01$ compared with the NT Mu-only group ($n = 12$ independent samples for treated groups). **e**, Representative staining of myofibres (labelled with F-actin) and cCasp3 (inset) 5, 10 and 15 d post-CTX injury in Q-VD-OPh-treated constructs. **f**, Tetanic force, muscle area (MA), cCasp3 area per nuclei (CaspA) and EdU+ cell density relative to values measured in Mu–BMDM constructs at 5, 10 and 15 d post-CTX. $^{\star}P < 0.05$ compared with the Mu–BMDM group for each separate measurement ($n = 6$ independent samples). The dashed line represents normalization to Mu–BMDM. All bars

and points denote means ± s.e.m. Significance was determined by two-way analysis of variance and post-hoc two-sided *t*-tests in **b** and **f**, and post-hoc Bonferroni-corrected two-sided *t*-tests in **d**. Supplementary Table 4 lists exact *P* values when greater than 0.0001.

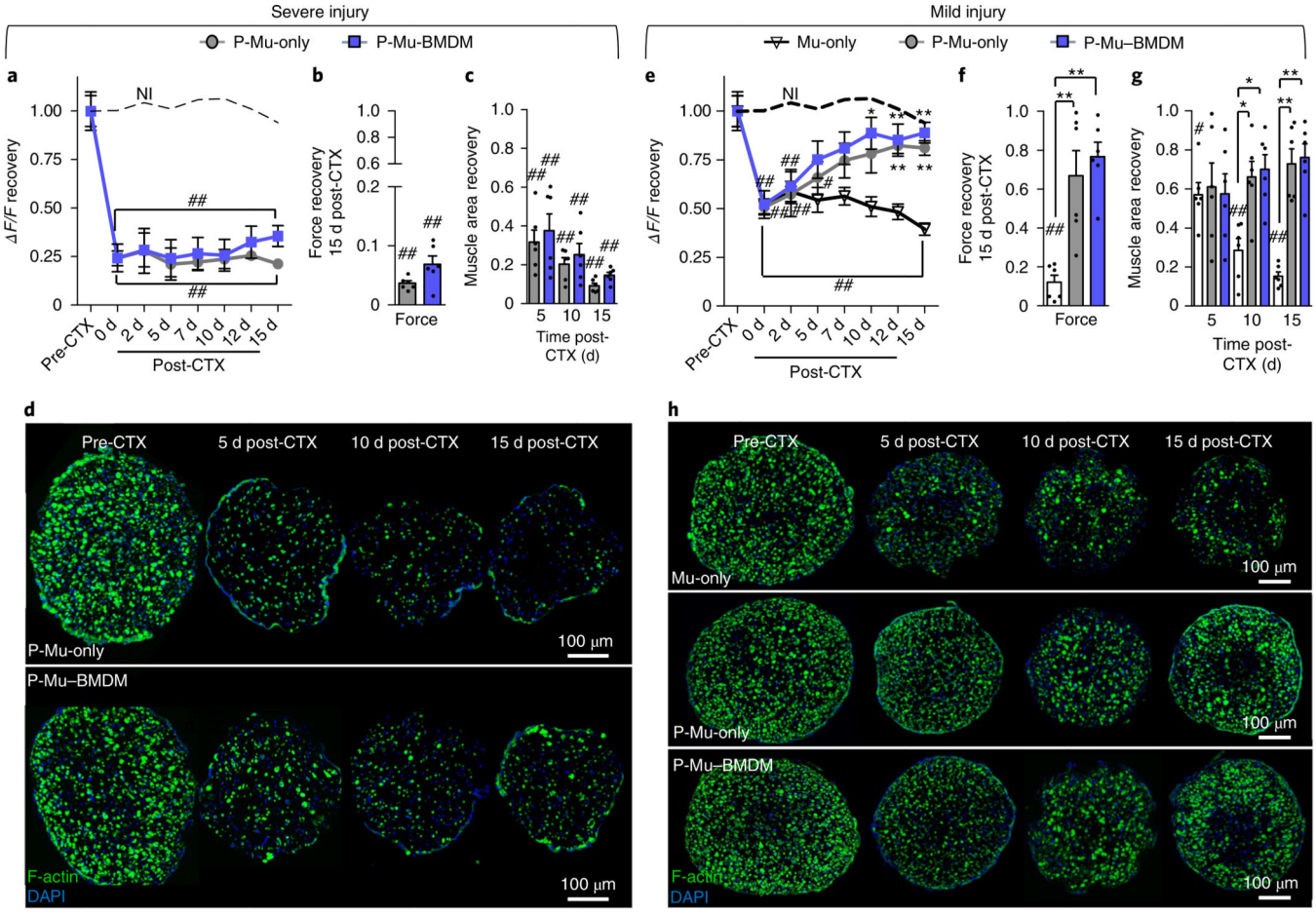

Fig. 5 |. In vitro regeneration of muscle constructs under shared-media conditions following CTX injury.

a,**e**, Plots of GCaMP6 signal ($\Delta F/F$) recovery with time post-injury (dashed lines represent non-injured (NI) Mu-only constructs) in P-Mu-only and P-Mu–BMDM constructs following severe (**a**) and mild (**e**) injury (Mu-only included in **e**). $^{\star}P < 0.05$ and $^{\star\star}P < 0.001$ compared with Mu-only constructs at the same time point (only in **e**); and $^{\#}P < 0.05$ and $^{\#\#}P < 0.001$ compared with NI Mu-only. The symbol dictating significance is designated to each point included within the brackets ($n = 12$ independent samples). **b**,**c**,**f**,**g**, Tetanic force generation at 15 d post-CTX (**b** and **f**) and muscle area recovery at 5, 10 and 15 d post-CTX (**c** and **g**) following severe (**b** and **c**) and mild (**f** and **g**) injury (Mu-only included in **f** and **g**). $^{\star}P < 0.05$ and $^{\star\star}P < 0.001$ at the same time point; and $^{\#}P < 0.05$ and $^{\#\#}P < 0.001$ relative to pre-CTX levels ($n = 6$ independent samples). **d**,**h**, Representative images of transverse cross-sections of muscle constructs showing myofibres (labelled with F-actin) at different times after severe (**d**) and mild (**h**) CTX-induced injury. All bars and points denote means ± s.e.m. Significance was determined by two-way analysis of variance and post-hoc Bonferroni-corrected two-sided *t*-tests in **a** and **e**, and two-sided *t*-test in **b**, **c**, **f** and **g**. Supplementary Table 4 lists exact *P* values when greater than 0.0001.

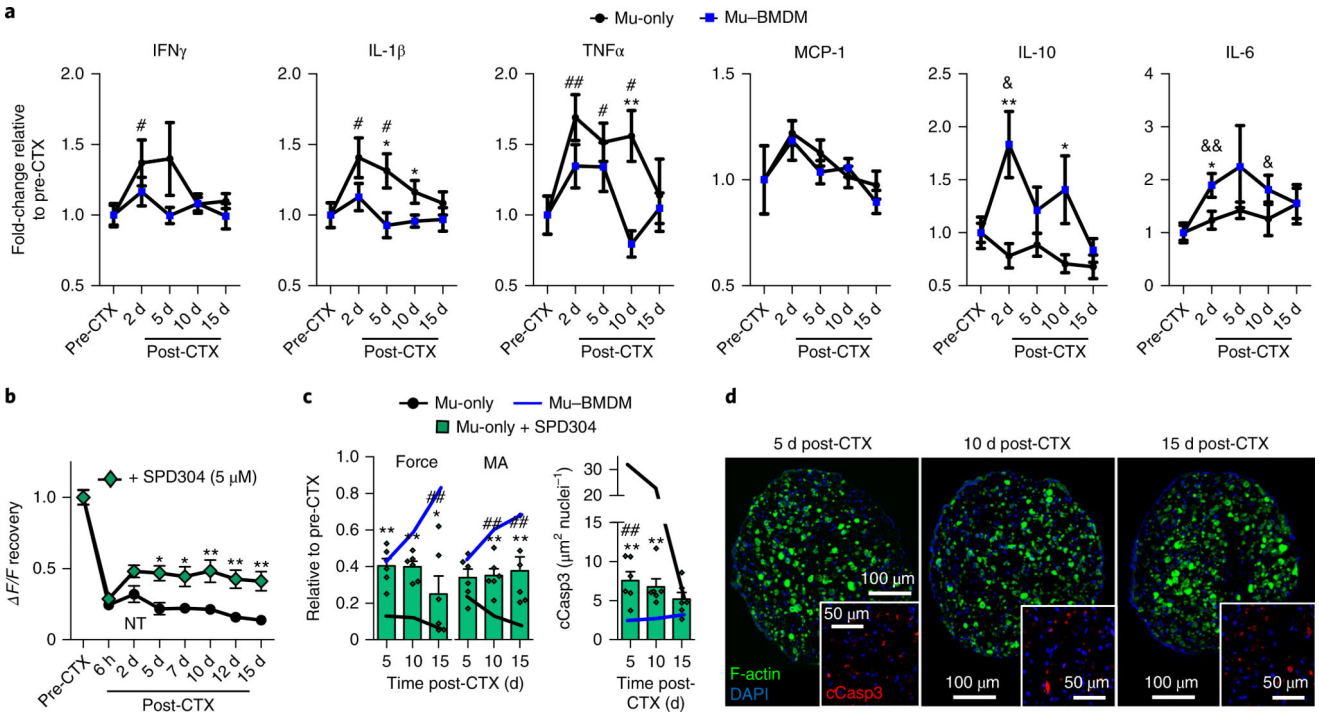

Fig. 6 |. Cytokine analysis following injury of engineered muscle and the effects of TNFα inhibition on recovery.

a, Cytokine concentrations relative to pre-injury levels in media conditioned by Mu-only and Mu–BMDM tissues pre-CTX and at 2, 5, 10 and 15 d post-CTX. $^{\star}P < 0.05$ and $^{\star\star}P < 0.01$ between groups at the same time point; and $^{\#}P < 0.05$ and $^{\#\#}P < 0.001$, and $^{\&}P < 0.05$ and $^{\&\&}P < 0.001$ compared with pre-CTX values in Mu-only and Mu–BMDM groups, respectively ($n = 12$ independent experiments). **b**, Plot of GCamp6 signal ($\Delta F/F$) recovery in Mu-only constructs exposed to the TNFα inhibitor SPD304. $^{\star}P < 0.05$ and $^{\star\star}P < 0.001$ compared with Mu-only constructs at same time point. The symbol dictating significance is designated to each point included within brackets ($n = 12$ independent samples). **c**, Plots of force and muscle area (MA) recovery (relative to pre-CTX values) and cleaved caspase-3 (cCasp3) area per nuclei in Mu-only constructs exposed to SPD304. $^{\star}P < 0.05$ and $^{\star\star}P < 0.001$ compared with Mu-only constructs at the same time point; and $^{\#\#}P < 0.001$ compared with Mu–BMDM constructs ($n = 6$ independent samples). **d**, Representative staining of cross-sections of myofibres and cCasp3 (inset) at 5, 10 and 15 d post-CTX in SPD304-treated constructs. All bars and points denote means ± s.e.m. Significance was determined by two-way analysis of variance and Bonferroni-corrected post-hoc two-sided *t*-tests. Supplementary Table 4 lists exact *P* values when greater than 0.0001.

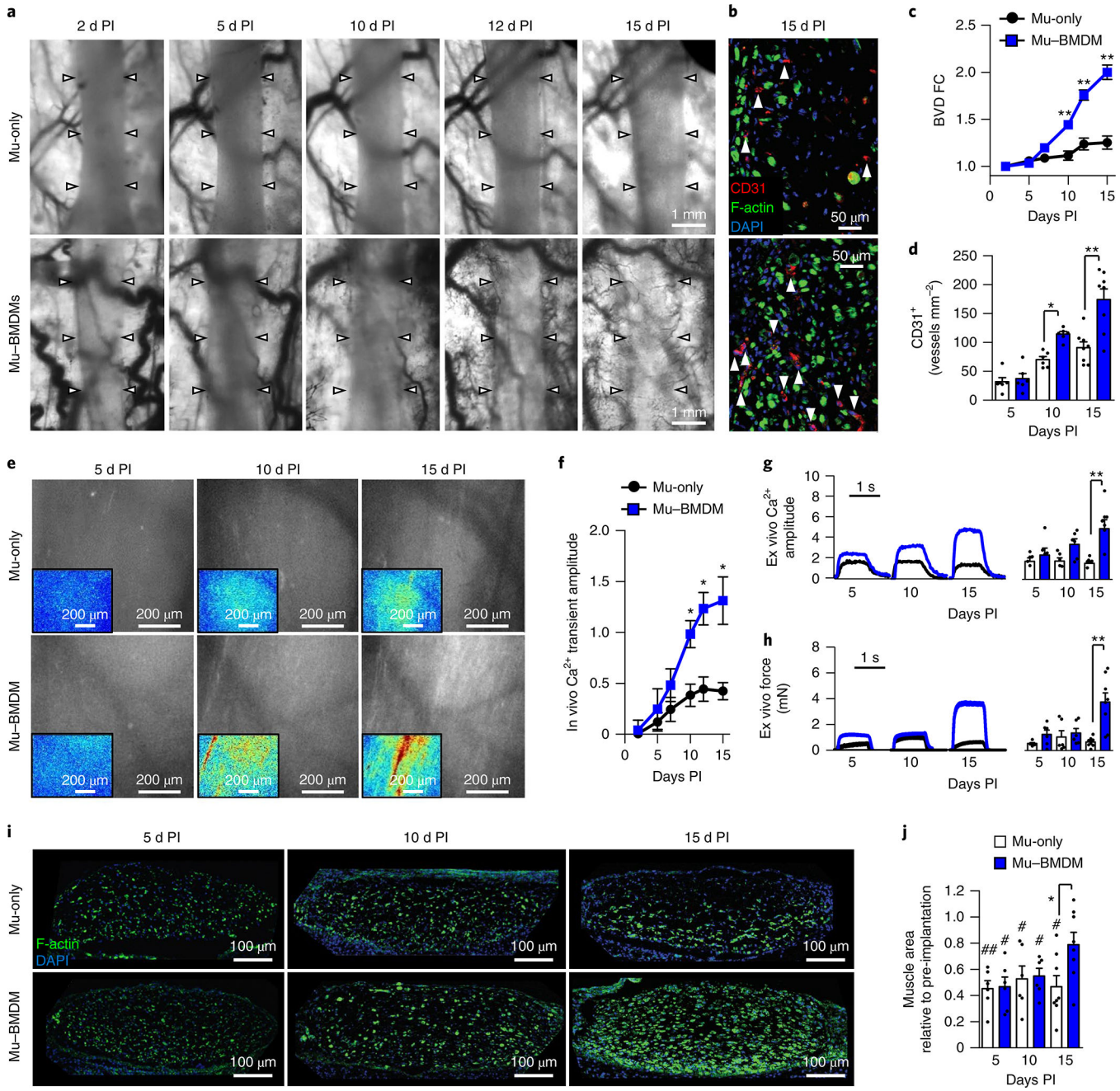

Fig. 7 |. Effect of BMdMs on implanted engineered muscle vascularization, function and survival.

a,b, Representative intravital images of vascular ingrowth over time (arrows specify the implant boundary) (**a**), and transverse cross-sections (**b**) of Mu-only and Mu–BMDM implants showing CD31+ vessels (marked by arrows) and myofibres (labelled with F-actin) 15 d post-implantation (PI). **c**,**d**, Quantification of blood vessel density fold-change (BVD FC) over 15 d PI (**c**) and cross-sectional lumen density at 5, 10 and 15 d PI (**d**). *$P <$ 0.05 and **$P <$ 0.001 compared with Mu-only at the same time point ($n =$ 6 for 5 and 10 d PI and $n =$ 8 for 15 d PI). **e**,**f**, Representative intravital images of peak spontaneous GCaMP6 signals in implanted Mu-only and Mu–BMDM constructs at days 5, 10 and 15 PI (**e**) (inset,

heat maps of $\Delta F/F$ with a consistent scale (blue, low values; red, high values)) and quantification of the Ca^{2+} transient amplitude ($\Delta F/F$) with time PI (**f**). $^{\star}P < 0.05$ between groups at specific time points. **g**,**h**, Representative ex vivo electrically induced traces (left) and quantified Ca^{2+} transient ($\Delta F/F$ of GCaMP6) (**g**) and tetanus force amplitudes (**h**) in Mu-only and Mu–BMDM explants at 5, 10 and 15 d PI. $^{\star\star}P < 0.001$ ($n = 6$ for 5 and 10 d PI and $n = 8$ for 15 d PI). **i**,**j**, Representative transverse cross-sections of Mu-only and Mu–BMDM implants showing myofibres labelled with F-actin (**i**), and quantification of the implant muscle area relative to pre-implantation values (**j**) at days 5, 10 and 15 PI. $^{*}P < 0.05$ between groups at specific time points; $^{\#}P < 0.05$ and $^{\#\#}P < 0.001$ compared with pre-implantation values ($n = 6$ for 5 and 10 d PI and $n = 8$ for 15 d PI). The dashed line represents normalization to pre-implantation. All bars and points denote means ± s.e.m. Significance was determined by two-way analysis of variance and post-hoc two-sided *t*-tests in **c**, **d** and **f**–**h**, and Tukey's multiple comparison post-hoc test in **j** (relative to pre-implantation). Supplementary Table 4 lists exact *P* values when greater than 0.0001.